Article

Cell Metabolism

# Mitochondrial calcium uptake declines during aging and is directly activated by oleuropein to boost energy metabolism and skeletal muscle performance

## Graphical abstract

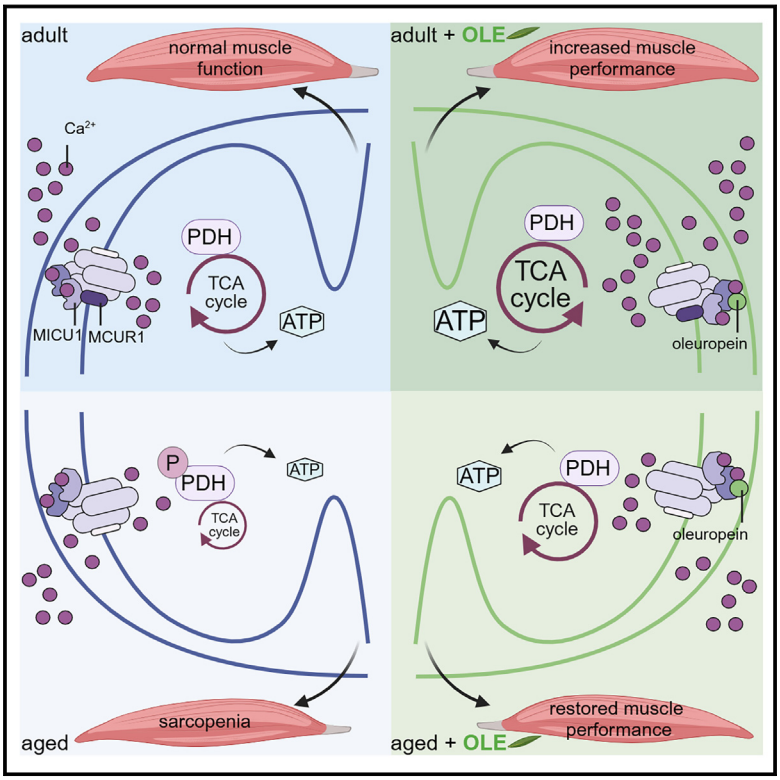


## Highlights

- Mitochondrial calcium uptake declines during muscle aging and sarcopenia via MCUR1
- The polyphenol oleuropein binds MICU1 to stimulate mitochondrial calcium import
- Oleuropein enhances muscle energy metabolism and exercise performance via MCU
- Oleuropein improves mitochondrial decline and muscle fatigue during aging

## Authors

Gaia Gherardi, Anna Weiser, Flavien Bermont, ..., Jerome N. Feige, Cristina Mammucari, Umberto De Marchi

## Correspondence

rosario.rizzuto@unipd.it (R.R.), jerome.feige@rd.nestle.com (J.N.F.), cristina.mammucari@unipd.it (C.M.), umberto.demarchi@rd.nestle.com (U.D.M.)

## In brief

Gherardi et al. identify that aging and disability impair mitochondrial calcium uptake in skeletal muscle via MCUR1. Food-derived polyphenols increase the import of calcium in mitochondria by binding MICU1. The natural MCU activator oleuropein stimulates energy metabolism, ameliorates muscle performance, and reverses age-related muscle decline by increasing mitochondrial calcium.

Gherardi et al., 2025, Cell Metabolism *37*, 1–19
February 4, 2025 
https://doi.org/10.1016/j.cmet.2024.10.021

CellPress

Cell Metabolism

CellPress
OPEN ACCESS

Article

# Mitochondrial calcium uptake declines during aging and is directly activated by oleuropein to boost energy metabolism and skeletal muscle performance

Gaia Gherardi,[1,13] Anna Weiser,[2,3,13] Flavien Bermont,[2] Eugenia Migliavacca,[2] Benjamin Brinon,[2] Guillaume E. Jacot,[2] Aurélie Hermant,[2] Mattia Sturlese,[4] Leonardo Nogara,[1,4] Filippo Vascon,[5] Agnese De Mario,[1] Andrea Mattarei,[4] Emma Garratt,[6,7] Mark Burton,[6] Karen Lillycrop,[6,7,8,15] Keith M. Godfrey,[6,7,9] Laura Cendron,[5] Denis Barron,[2] Stefano Moro,[4] Bert Blaauw,[1,10] Rosario Rizzuto,[1,11,14,*] Jerome N. Feige,[2,12,14,16,*] Cristina Mammucari,[1,11,14,*] and Umberto De Marchi[2,14,*]

[1]Department of Biomedical Sciences, University of Padova, 35131 Padova, Italy
[2]Nestlé Institute of Health Sciences, Nestlé Research, Société des Produit Nestlé S.A., EPFL Innovation Park, 1015 Lausanne, Switzerland
[3]Molecular Nutritional Medicine, Else Kröner Fresenius Center for Nutritional Medicine, Technische Universität München, 85354 Freising, Germany
[4]Molecular Modeling Section (MMS), Department of Pharmaceutical and Pharmacological Sciences, University of Padova, via Marzolo 5, 35131 Padova, Italy
[5]Department of Biology, University of Padova, 35131 Padova, Italy
[6]Human Development and Health Academic Unit, Faculty of Medicine, University of Southampton, Southampton, UK
[7]NIHR Southampton Biomedical Research Centre, University of Southampton & University Hospital Southampton NHS Foundation Trust, Southampton, UK
[8]Biological Sciences, Faculty of Environmental and Life Sciences, University of Southampton, Southampton, UK
[9]Medical Research Council Lifecourse Epidemiology Centre, University of Southampton, Southampton, UK
[10]Venetian Institute of Molecular Medicine (VIMM), Via Orus 2, 35129 Padova, Italy
[11]Myology Center (CIR-Myo), University of Padova, 35131 Padova, Italy
[12]School of Life Sciences, Ecole Polytechnique Fédérale de Lausanne (EPFL), Lausanne, Switzerland
[13]These authors contributed equally
[14]These authors contributed equally
[15]Deceased
[16]Lead contact
*Correspondence: rosario.rizzuto@unipd.it (R.R.), jerome.feige@rd.nestle.com (J.N.F.), cristina.mammucari@unipd.it (C.M.), umberto.demarchi@rd.nestle.com (U.D.M.)
https://doi.org/10.1016/j.cmet.2024.10.021

## SUMMARY

Mitochondrial calcium ($mtCa^{2+}$) uptake via the mitochondrial calcium uniporter (MCU) couples calcium homeostasis and energy metabolism. $mtCa^{2+}$ uptake via MCU is rate-limiting for mitochondrial activation during muscle contraction, but its pathophysiological role and therapeutic application remain largely uncharacterized. By profiling human muscle biopsies, patient-derived myotubes, and preclinical models, we discovered a conserved downregulation of mitochondrial calcium uniporter regulator 1 (MCUR1) during skeletal muscle aging that associates with human sarcopenia and impairs $mtCa^{2+}$ uptake and mitochondrial respiration. Through a screen of 5,000 bioactive molecules, we identify the natural polyphenol oleuropein as a specific MCU activator that stimulates mitochondrial respiration via mitochondrial calcium uptake 1 (MICU1) binding. Oleuropein activates $mtCa^{2+}$ uptake and energy metabolism to enhance endurance and reduce fatigue in young and aged mice but not in muscle-specific MCU knockout (KO) mice. Our work demonstrates that impaired $mtCa^{2+}$ uptake contributes to mitochondrial dysfunction during aging and establishes oleuropein as a novel food-derived molecule that specifically targets MCU to stimulate mitochondrial bioenergetics and muscle performance.

## INTRODUCTION

Cellular energy production relies in large part on oxidative metabolism and ATP synthesis in mitochondria. Mitochondrial dysfunction is a major hallmark of aging that contributes to physiological decline and chronic diseases during aging.[1,2] The anti-diabetic drug metformin is being clinically tested to target aging, given its geroprotective effects on lifespan and healthspan that act, at least in part, by triggering mitochondrial adaptations via mitohormesis.[3] Other clinical therapeutic molecules such as

Please cite this article in press as: Gherardi et al., Mitochondrial calcium uptake declines during aging and is directly activated by oleuropein to boost energy metabolism and skeletal muscle performance, Cell Metabolism (2024), https://doi.org/10.1016/j.cmet.2024.10.021



nicotinamide adenine dinucleotide (NAD)$^+$ precursors,[4–7] autophagy/mitophagy activators,[8–10] and mitochondrial complex stabilizers[11,12] can prevent age-related decline indirectly by targeting other hallmarks of aging that maintain mitochondrial integrity and rewire bioenergetics during aging. In contrast, there are no approved therapeutics that directly stimulate the core ATP-generating bioenergetic capacity of mitochondria.

Mitochondrial metabolism is particularly important in skeletal muscle, where contraction during physical activity is an extremely demanding process that consumes massive amounts of cellular energy.[13] Exercise maintains mitochondrial fitness in muscle during aging,[14] and mitochondrial dysfunction is a major contributor to the age-related decline of skeletal muscle.[15–18] Low mitochondrial activity of all respiratory complexes directly contributes to low muscle mass, low muscle strength, and low walking speed[15,19,20]—the clinical features of sarcopenia that impact physical autonomy, quality of life, and mortality.[21] The medical management of sarcopenia relies on lifestyle interventions with exercise and nutrition.[22] Although recent large clinical studies have demonstrated the benefits of structured exercise programs,[23–25] nutritional management of sarcopenia largely relies on restoring the nutritional deficits of older adults in protein and micronutrients.[21,26,27] Polyphenol-rich diets, including Mediterranean diets rich in olive oil, have also been associated with lower risk of chronic diseases of aging, in particular cardiovascular diseases.[28,29] However, the nature and mechanisms of the individual polyphenols mediating these health benefits remain elusive, and the role of polyphenols in sarcopenia remains to be explored.

The regulation of mitochondrial calcium (mtCa$^{2+}$) directly controls oxidative metabolism and regulates skeletal muscle physiology.[30,31] The uptake of calcium in mitochondria is controlled by the mitochondrial calcium uniporter (MCU), a multi-proteic complex composed of the MCU channel that transports Ca$^{2+}$ across the inner mitochondrial membrane, and of regulatory subunits that regulate MCU activity to adapt to the metabolic requirements of the cell.[32–34] During excitation-contraction coupling, Ca$^{2+}$ is released from the sarcoplasmic reticulum (SR) to stimulate contraction, and mtCa$^{2+}$ couples the metabolic needs of contraction to ATP production via mitochondrial oxidative metabolism. Mechanistically, this is controlled by the activation of dehydrogenases of the tricarboxylic acid (TCA) cycle that are regulated by mtCa$^{2+}$ levels. In particular, activation of the rate-limiting pyruvate dehydrogenase (PDH) occurs upon dephosphorylation by the Ca$^{2+}$-dependent PDH phosphatase 1 (PDP).

Increased mtCa$^{2+}$ and MCU activity in skeletal muscle has recently been linked to mitochondrial adaptations in response to different types of exercise training in humans.[35] Stimulating mtCa$^{2+}$ uptake is sufficient to drive some of these adaptations, as skeletal muscle overexpression of MCU in mice also promotes mitochondrial metabolism and structural muscle adaptations.[36] Conversely, mtCa$^{2+}$ uptake is rate-limiting for normal muscle metabolism and contractile function, with genetic deletion of MCU in skeletal muscle impairing mitochondrial oxidative capacity and reducing muscle force and exercise performance.[31,36] In addition, regulatory subunits of the MCU complex fine-tune muscle physiology, as skeletal-muscle-specific deletion of mitochondrial calcium uptake 1 (MICU1) compromises mtCa$^{2+}$ uptake and energy metabolism, leading to myofiber damage and muscle weakness and fatigue.[37] Human genetics have also confirmed a central role of mtCa$^{2+}$ uptake via the MCU complex in muscle physiology.[38] Monogenic mutations of MICU1 cause rare orphan diseases with myopathic phenotypes[39] that present with severe fatigue and lethargy.[40] Although these studies collectively highlight a robust link between mtCa$^{2+}$ regulation and skeletal muscle health, the role of MCU in chronic conditions such as muscle wasting disorders and aging is not well understood, and translatable therapeutic tools and interventions to boost mtCa$^{2+}$ by activating MCU are lacking.

Here, we discovered that the capacity for mtCa$^{2+}$ uptake declines during aging in model organisms and in humans via downregulation of mitochondrial calcium uniporter regulator 1 (MCUR1), and cellular and *in vivo* genetic rescue experiments demonstrated that reduced MCUR1 directly contributes to impaired mitochondrial energy metabolism. To overcome this, we screened 5,000 natural bioactive molecules present in food and discovered the oleuropein olive polyphenol as a potent and selective activator of MCU, with therapeutic potential for skeletal muscle. Oleuropein stimulates mtCa$^{2+}$ uptake via direct binding of its deglycosylated metabolite to the MICU1 subunit of MCU, inducing acute ergogenic effects and chronic adaptations to increase oxidative metabolism and muscle performance *in vivo*. Oleuropein also overcomes the age-related MCUR1-dependent impairment of mtCa$^{2+}$ and rescues mitochondrial activity and physical performance in aged mice. Our work establishes the regulation of MCU-dependent mtCa$^{2+}$ uptake as a novel mechanism of aging and demonstrates that oleuropein is a first-in-class natural molecule to enhance muscle performance and prevent muscle aging by directly activating MCU and mitochondrial bioenergetics with high specificity.

## RESULTS

### mtCa$^{2+}$ uptake declines during aging and sarcopenia in human skeletal muscle via downregulation of MCUR1

Given the regulation of mitochondrial bioenergetics by mtCa$^{2+}$ and the role of mitochondrial dysfunction in driving aging of skeletal muscle, we investigated whether mtCa$^{2+}$ participates in the pathophysiology of muscle aging. MtCa$^{2+}$ uptake was compared in primary human myotubes (Figure 1A) from adult and aged donors, where the ryanodine receptor (RyR1) was stimulated with caffeine to mimic contraction-induced Ca$^{2+}$ release from the SR. The capacity of skeletal muscle mitochondria to take up Ca$^{2+}$ was strongly impaired by aging, as mtCa$^{2+}$ uptake was reduced by 45% in aged individuals (Figures 1B and 1C).

We then evaluated whether the severity of age-related muscle decline impacts mtCa$^{2+}$ by comparing primary myotubes from healthy older people and from sarcopenic patients that have low muscle mass and function defined by the clinical diagnosis criteria of sarcopenia (Figure S1A). MtCa$^{2+}$ uptake was significantly lower in myotubes from sarcopenic donors than in myotubes from healthy older people (Figures S1B and S1C), demonstrating that pathological muscle aging exacerbates dysfunctional mtCa$^{2+}$ uptake. To characterize the molecular mechanisms underlying these defects, we analyzed the expression of genes controlling mtCa$^{2+}$ uptake and extrusion in human muscle biopsies from older people with sarcopenia.[15] Sarcopenia significantly reduced the expression of *MCUR1* (Figure 1D), a regulator of mtCa$^{2+}$ transport,[41–45] whereas other genes

Please cite this article in press as: Gherardi et al., Mitochondrial calcium uptake declines during aging and is directly activated by oleuropein to boost energy metabolism and skeletal muscle performance, Cell Metabolism (2024), https://doi.org/10.1016/j.cmet.2024.10.021



CellPress
OPEN ACCESS

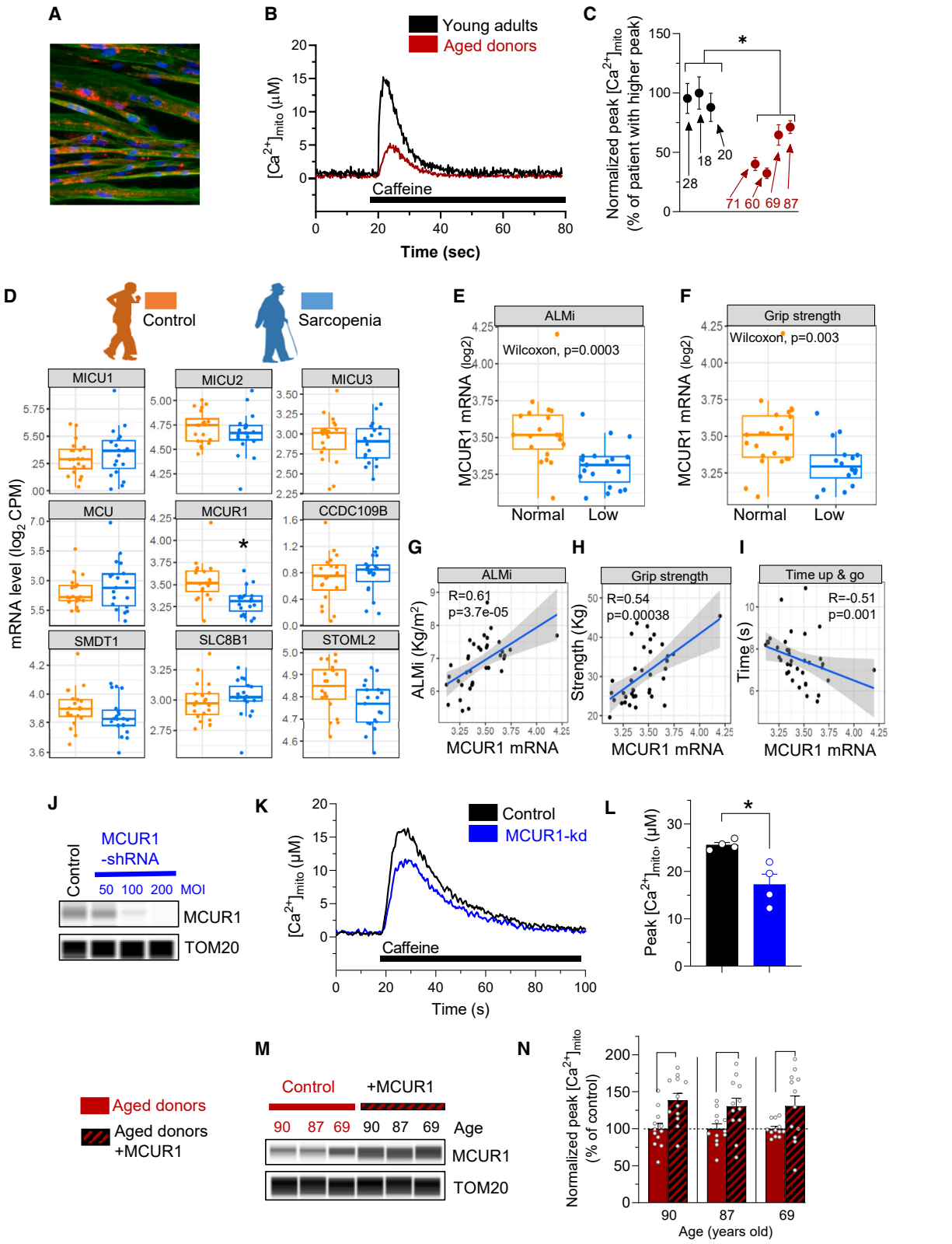


*(legend on next page)*

regulating $mtCa^{2+}$ were not altered. Pathway and interactome analyses confirmed that decreased *MCUR1* expression in sarcopenia controls a molecular node regulating $mtCa^{2+}$ homeostasis via the MCU (Figure S1D). Downregulation of *MCUR1* was linked to both low muscle mass, assessed via appendicular lean mass index (ALMi) by DXA (Figure 1E), and muscle strength assessed by grip strength (Figure 1F). In continuous variable analysis, the muscle expression of *MCUR1* also positively associated with ALMi, grip strength, and gait speed (Figures 1G, 1H, and S1E) and negatively associated with the time required to perform a "time-up-and-go" or chair rise test (Figures 1I and S1F), all indicative that *MCUR1* expression is high in elderly people with high physical capacity. These results demonstrate that the regulation of $mtCa^{2+}$ transport is altered in human skeletal muscle during aging and physical decline and suggest a possible role of *MCUR1* in mediating the age-related impairment of $mtCa^{2+}$ uptake.

To test whether the downregulation of *MCUR1* observed during sarcopenia can impair skeletal muscle $mtCa^{2+}$ uptake, we depleted *MCUR1* in primary human myotubes from young adults using viral short hairpin RNA (shRNA) expression (Figure 1J). *MCUR1* knockdown (kd) reduced $mtCa^{2+}$ uptake after caffeine stimulation by 33% (Figures 1K and 1L), demonstrating that the downregulation of *MCUR1* is sufficient to recapitulate the effects of aging on $mtCa^{2+}$ uptake (Figures 1B and 1C). We then tested whether decreased MCUR1 contributes to impaired $mtCa^{2+}$ uptake during aging by over-expressing MCUR1 in human myotubes from aged donors (Figure 1M). *MCUR1* overexpression stimulated $mtCa^{2+}$ uptake in myotubes from all aged donors tested, from 69 to 90 years of age (Figure 1N), demonstrating that decreased skeletal muscle *MCUR1* expression is a cause of impaired $mtCa^{2+}$ uptake during aging.

Taken together, these results demonstrate that a downregulation of *MCUR1* causally contributes to a progressive impairment of $mtCa^{2+}$ uptake during physiological and pathological skeletal muscle aging.

## Impaired $mtCa^{2+}$ uptake alters PDH activity and energy metabolism in a preclinical model of natural aging

To investigate whether the regulation of $mtCa^{2+}$ homeostasis occurring during human aging can be modeled preclinically, we analyzed $mtCa^{2+}$ uptake and expression of genes regulating $mtCa^{2+}$ uptake in the skeletal muscle of mice aged 24 months compared with young controls. As previously reported,[46] cytosolic $Ca^{2+}$ transients generated upon caffeine stimulation were decreased in *aged* myofibers, whereas resting cytosolic $Ca^{2+}$ levels were unaltered (Figures S2A and S2B). $MtCa^{2+}$ uptake, measured in isolated mouse myofibers upon caffeine-induced $Ca^{2+}$ release, decreased during aging (Figures 2A and 2B), whereas resting $mtCa^{2+}$ levels were unaltered (Figure 2C). Similar to what was observed during human muscle aging, the regulation of MCU subunits directly contributed to this phenotype, as *MCUR1* was downregulated by 54% during natural mouse aging, whereas the expression of the channel (*MCU*, *MCUb*, and *EMRE*) and of other regulatory subunits (*MICU1*, *MICU1.1*, *MICU2*, and *MICU3*) were unaltered in aged mice (Figures 2D and S2C). As schematized in Figure 2E, mitochondrial matrix $Ca^{2+}$ acutely activates PDH via dephosphorylation mediated by allosteric activation of the $Ca^{2+}$-dependent PDP. We previously demonstrated that decreased $mtCa^{2+}$ uptake triggered by a muscle-specific deletion of *MCU* ($skMCU^{-/-}$) reduces PDH activity, impairs mitochondrial oxygen consumption rate (OCR), and rewires substrate dependency from glucose to fatty acid oxidation,[31] all in a PDP-dependent fashion as *PDP* overexpression is sufficient to restore these phenotypes.[31] We hypothesized that the reduction in $mtCa^{2+}$ uptake observed during skeletal muscle aging could trigger similar metabolic impairments. PDH phosphorylation levels, which inversely correlate with PDH activity, increased by 54% in aged muscle (Figures 2F and 2G), and basal, ATP-dependent, and maximal OCR measured in isolated myofibers declined in the muscle of aged mice (Figures 2H and 2I). Inhibition of fatty acid oxidation with etomoxir had a greater impact on OCR in aged muscle, demonstrating that aging shifts the substrate preference of mitochondria toward fatty acid (FA) oxidation (Figures 2J and 2K).

To test whether the impaired MCU activity contributes to mitochondrial dysfunction during aging, we first performed genetic *in vivo* overexpression of MCUR1 in skeletal muscle of young and aged mice. MCUR1 overexpression had no effect in young healthy muscle but reversed the decline of mitochondrial respiration in aged muscle (Figure 2L), specifically in conditions where *MCUR1* expression is reduced (Figure 2D). We then used a parallel pharmacological strategy where the PDH complex was activated by inhibition of pyruvate dehydrogenase kinase

**Figure 1. Uptake of mitochondrial calcium declines during aging in human skeletal muscle**

(A–C) Aequorin-based $mtCa^{2+}$ uptake in primary human myotubes from aged vs. young donors. (A) Primary human myoblasts differentiated in myotubes and immunostained for fibers (troponin-t, green), mitochondria (MCU, red), and nuclei (DAPI, blue). Representative $mtCa^{2+}$ traces (B) and quantification of the $mtCa^{2+}$ uptake peak (C) in myotubes from young and aged donors ($n > 5$ samples/donor).

(D) mRNA expression of genes regulating $mtCa^{2+}$ measured by RNA sequencing of human skeletal muscle biopsies of sarcopenic vs. age-matched healthy older people ($n = 19–20$ muscle samples/group; CPM, counts per million).

(E and F) MCUR1 mRNA expression in skeletal muscle biopsies of older people with low appendicular lean mass index (*ALMI*, E) or low grip strength (F).

(G–I) Correlation of MCUR1 mRNA expression in skeletal muscle biopsies of older people with ALMI (G), grip strength (H), and performance in the "time-up-and-go" test (I).

(J–L) MCUR1 knockdown (MCUR1-kd) decreases $mtCa^{2+}$ uptake during 5 mM caffeine stimulation. (J) Validation of MCUR1 protein expression by capillary western blot after MCUR1-kd using adenoviral-infection-mediated shRNA delivery in primary human myotubes. Scramble shRNA was used as control and TOM20 was used as the internal standard of mitochondrial content. MOI, multiplicity of infection. (K) Representative $mtCa^{2+}$ traces after MCUR1-kd in primary human myotubes. (L) Quantification of the effect of MCUR1-kd on $mtCa^{2+}$ uptake peak, after 5 mM caffeine stimulation.

(M and N) Re-expression of *MCUR1* in human myotubes of aged donors. (M) Validation of MCUR1 protein expression in human myotubes of aged donors after adenoviral overexpression. (N) $mtCa^{2+}$ uptake in primary human myotubes from aged donors after *MCUR1* overexpression. $n = 13$ cellular replicates/condition from 2 independent experiments.

In all bar graphs, data are presented as mean ± SEM with $^*p < 0.05$ using a two-tailed unpaired t test.

Please cite this article in press as: Gherardi et al., Mitochondrial calcium uptake declines during aging and is directly activated by oleuropein to boost energy metabolism and skeletal muscle performance, Cell Metabolism (2024), https://doi.org/10.1016/j.cmet.2024.10.021



CellPress
OPEN ACCESS

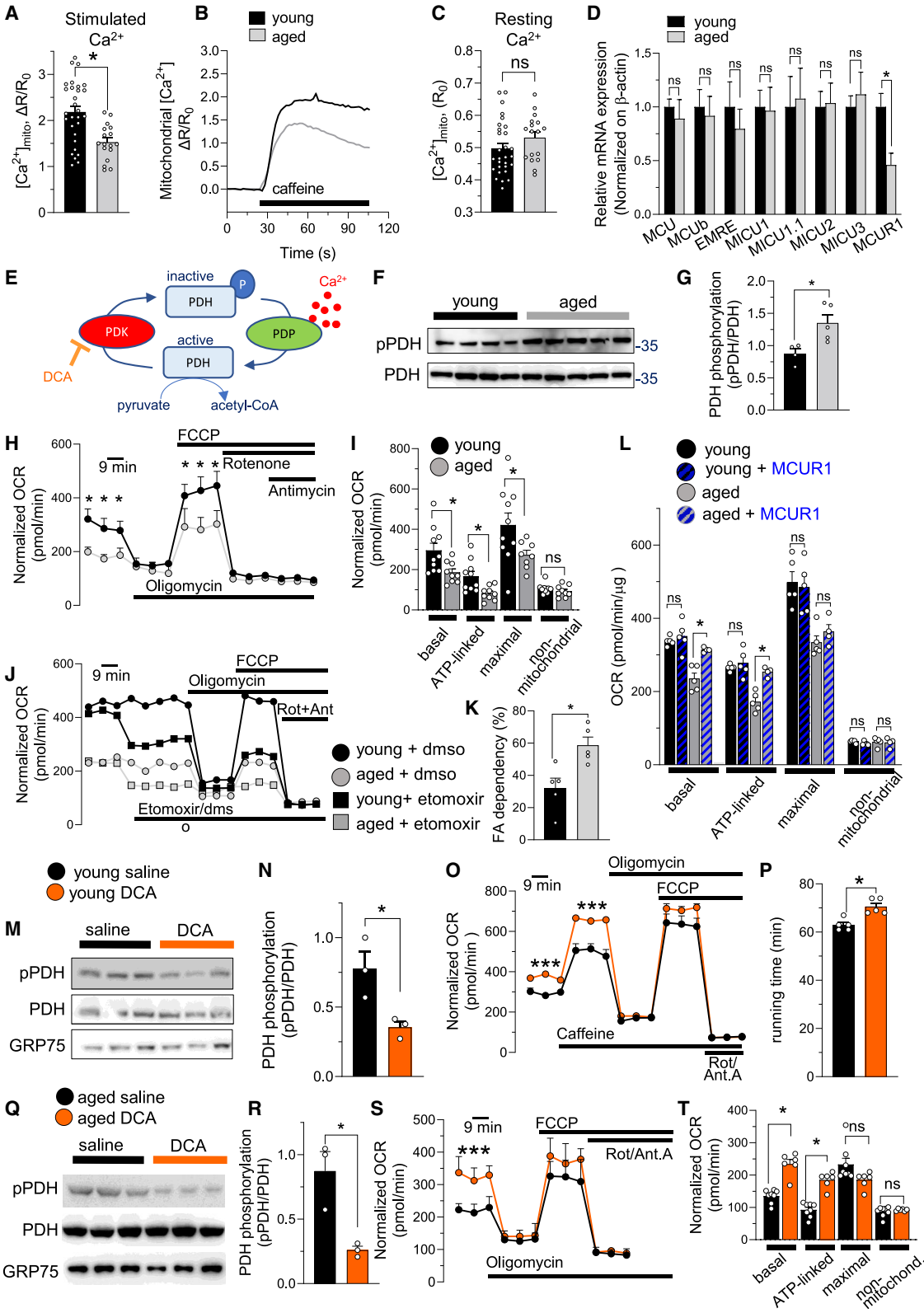


**Figure 2. Impaired mitochondrial calcium uptake during aging impairs energy metabolism via PDH in skeletal muscle**

(A–C) Mt-fura-2-based mtCa$^{2+}$ measurement of flexor digitorum brevis (FDB) myofibers from aged vs. young mice. Quantification (A) and representative traces (B) of peak mtCa$^{2+}$ uptake upon 30-mM caffeine stimulation, and resting mtCa$^{2+}$ levels (C) ($n$ > 20 fibers from 3 mice/group).

*(legend continued on next page)*

Please cite this article in press as: Gherardi et al., Mitochondrial calcium uptake declines during aging and is directly activated by oleuropein to boost energy metabolism and skeletal muscle performance, Cell Metabolism (2024), https://doi.org/10.1016/j.cmet.2024.10.021



(PDK) by dichloroacetate (DCA) (Figure 2E), as previously used to link increased oxidative phosphorylation activity and muscle strength in a mouse model of amyotrophic lateral sclerosis.[47] We used *in vivo* DCA treatment to test whether boosting PDH activity could also stimulate metabolism and performance of young healthy mice or rescue the consequences of impaired genetic or age-related $mtCa^{2+}$ uptake. In young mice, DCA treatment stimulated muscle PDH by reducing its phosphorylation (Figures 2M and 2N), increased myofiber respiration (Figure 2O), and boosted endurance exercise performance (Figure 2P). DCA could overcome impaired mitochondrial bioenergetics caused by genetically altered $mtCa^{2+}$ uptake as OCR increased and FA dependency decreased in $skMCU^{-/-}$ myofibers treated with DCA (Figures S2D and S2E). Finally, DCA treatment in aged animals decreased PDH phosphorylation (Figures 2Q and 2R) and increased basal and ATP-linked OCR (Figures 2S and 2T). These results indicate that the MCU-PDH axis declines in aged muscle via a mechanism that involves MCUR1 and that restoring PDH activity overcomes the bioenergetic defects caused by impaired $mtCa^{2+}$ uptake during aging.

## A HT screen identifies the natural polyphenol oleuropein as a potent activator of mitochondrial calcium uptake

Given the link of $mtCa^{2+}$ uptake with mitochondrial energy metabolism and muscle performance and its impairment during skeletal muscle aging, we performed a high-throughput (HT) screen of natural molecules that activate $mtCa^{2+}$ to identify novel nutritional solutions that could stimulate mitochondrial bioenergetics and reverse age-related decline (Figures S3A and S3B). We analyzed 5,571 natural molecules present in food on $mtCa^{2+}$ uptake in HeLa cells stimulated with histamine (Figures 3A, 3B, and S3C), using kaempferol as a positive control.[48] 78 primary hits, corresponding to a rate of 1.4% positive hits (Figures 3A and 3B), were filtered by orthogonal screening (Figure 3C) and the resulting 52 positive hits were counter-screened for their ability to specifically increase $mtCa^{2+}$ without triggering cytosolic $Ca^{2+}$ rise (Figure 3D). By filtering the 43 molecules that specifically and reproducibly activate $mtCa^{2+}$ for known safety and bioavailability in humans, we identified that the olive polyphenol oleuropein has the best profile of bioactive and safe $mtCa^{2+}$ activation (Figure 3E; Clewell et al.[49]). We confirmed the effect of oleuropein in intact cells as a specific mitochondrial (Figures 3F and 3G), and not cytosolic, $Ca^{2+}$ activator (Figure 3H). In addition, oleuropein also increased $mtCa^{2+}$ uptake in semi-permeabilized HeLa cells stimulated with exogenous $Ca^{2+}$ to override $Ca^{2+}$ release from the reticulum (Figure 3I), demonstrating that oleuropein stimulates $mtCa^{2+}$ uptake via a direct effect on MCU activity, but not indirect modulation, of intracellular $Ca^{2+}$ storage, release, or influx from the SR. Two recent studies have suggested that small molecules that regulate $mtCa^{2+}$ uptake may interact with the MICU1 protein via *in silico* modeling.[50,51] Given the optimal position of MICU1 for interactions with molecules that diffuse from the cytoplasm to the mitochondrial intermembrane space, along with its ability to interact with ligands,[50] we conducted surface plasmon resonance (SPR) experiments to directly assess the binding of oleuropein to purified MICU1 *in vitro*. These measurements revealed that oleuropein binds to MICU1 with low micromolar affinity ($K_D$ of 4 ± 1 μM) (Figures 3J and S3D).

Because oleuropein is a glycosylated molecule that is metabolized upon intestinal absorption (Figure 3K; Clewell et al.[49]), we also tested the ability of oleuropein and its secondary metabolites to promote mitochondrial calcium uptake in dose response (Figures 3L–3N). Oleuropein dose-dependently activated $mtCa^{2+}$ uptake with a cellular EC50 of 10 μM (Figure 3L). Metabolites were also biologically active on stimulated $mtCa^{2+}$ uptake, with oleuropein aglycone (oleuropein-a) being the most potent metabolite, with an EC50 of 5 μM (Figure 3M), and the secondary metabolite hydroxytyrosol having weaker potency and affinity (Figure 3N). The cellular EC50 of oleuropein and its metabolites on $mtCa^{2+}$ uptake were in the same range as its *in vitro* $K_D$ for MICU1 (Figure 3J). These results demonstrate that oleuropein and its direct metabolites are potent and direct activators of $mtCa^{2+}$ uptake, with a favorable safety and bioavailability for human clinical use.

## Oleuropein requires MICU1 to stimulate MCU-dependent mitochondrial energy metabolism in primary human myotubes

Given the role of $mtCa^{2+}$ in coupling contraction with energy production in skeletal muscle, we investigated whether oleuropein also enhances $mtCa^{2+}$ and energy metabolism in models of

(D) Relative mRNA expression levels of MCU complex genes in tibialis anterior (TA) muscles from aged vs. young mice ($n$ = 5 mice/group).
(E) Representative scheme of PDH regulation. $Ca^{2+}$ binding in the mitochondrial matrix activates pyruvate dehydrogenase phosphatase 1 (PDP1), the $Ca^{2+}$-dependent isoform of the PDP enzyme that, in turn, dephosphorylates and activates PDH, leading to acetyl-coenzyme A (CoA) production. Dichloroacetate (DCA) inhibits PDK.
(F and G) PDH phosphorylation levels quantified by western blot in aged TA muscles from aged vs. young mice ($n$ = 4–5 mice/group).
(H and I) Oxygen consumption rate (OCR) in isolated FDB myofibers from aged vs. young mice. Data are normalized on mean calcein fluorescence (H) and components of respiration accounting for basal, ATP-dependent (quantified after oligomycin treatment), maximal (quantified after carbonyl cyanide-p-trifluoromethoxyphenylhydrazone [FCCP] treatment), and non-mitochondrial (quantified after rotenone + antimycin treatment) respiration are quantified in (I) ($n$ = 10 samples/group).
(J and K) Fatty acid (FA)-dependent respiration measured in FDB myofibers from aged vs. young mice. Etomoxir was used to inhibit FA utilization (J). FA dependency was calculated and expressed as the etomoxir-sensitive percentage of basal OCR (K). Data are normalized on mean calcein fluorescence ($n$ = 5 samples/group).
(L) OCR in isolated FDB myofibers from aged vs. young mice with *in vivo* overexpression of MCUR1. Normalization and description of the respiration component as described in (I). $n$ = 4 samples/group.
(M–T) Effects of DCA-mediated PDH activation in skeletal muscle of young (M–P) and aged (Q–T) mice. (M, N, Q, and R) PDH phosphorylation levels quantified by western blot in TA muscles of DCA-treated mice compared with saline controls using GRP75 as loading control; $n$ = 3 mice/group. (O, S, and T) OCR measured in FDB myofibers and normalized on mean calcein fluorescence in DCA-treated mice compared with saline controls ($n$ = 6–10 samples/group). (P) Exercise performance assessed by maximal treadmill running time in DCA-treated mice compared with saline controls ($n$ = 5 mice/group).
In all bar graphs, data are presented as mean ± SEM with $^*p < 0.05$ using a two-tailed unpaired t test, except in (J), where a one-way ANOVA was applied.

Please cite this article in press as: Gherardi et al., Mitochondrial calcium uptake declines during aging and is directly activated by oleuropein to boost energy metabolism and skeletal muscle performance, Cell Metabolism (2024), https://doi.org/10.1016/j.cmet.2024.10.021



CellPress
OPEN ACCESS

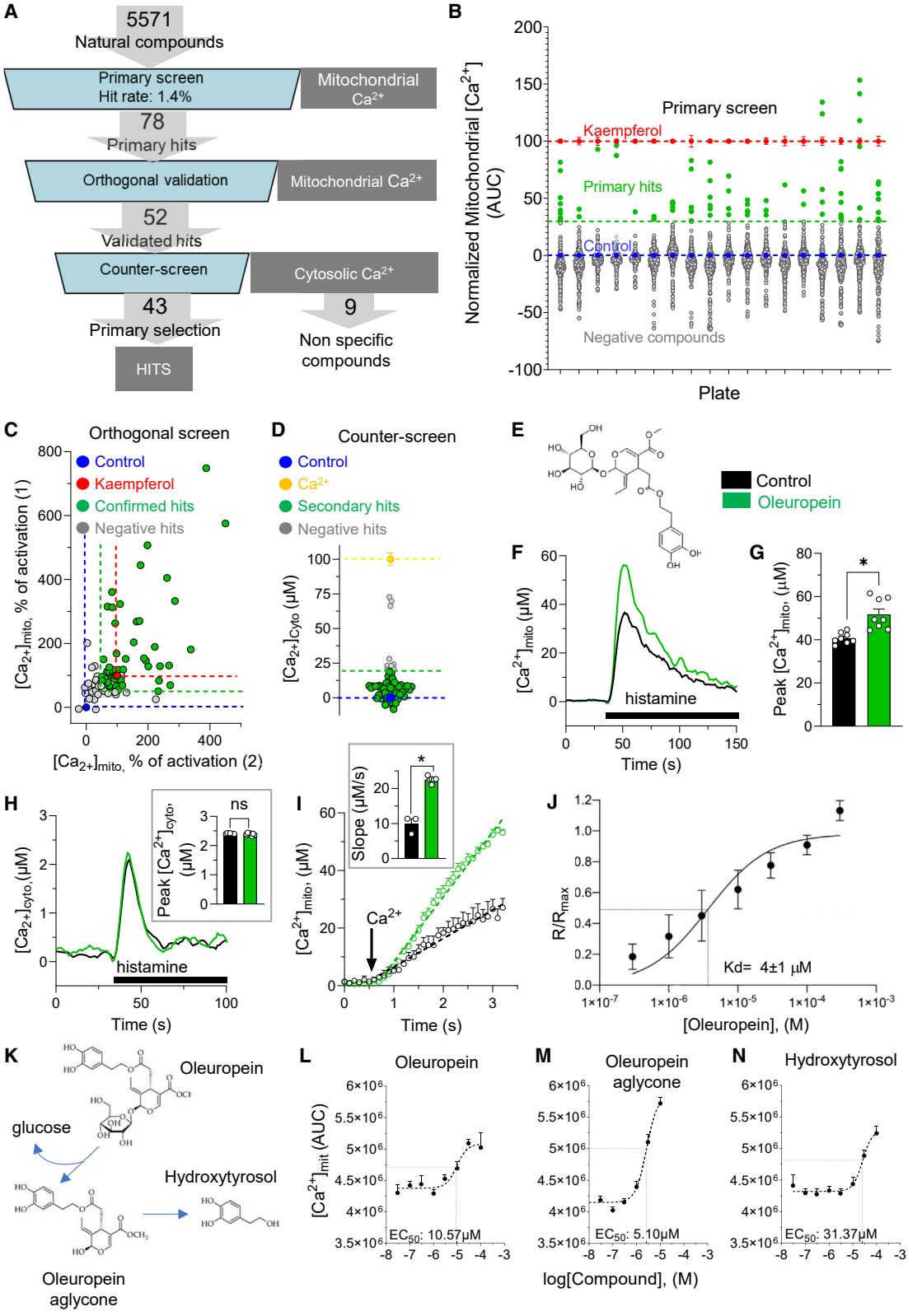


**Figure 3. A high-throughput screen identifies the natural polyphenol oleuropein as a potent activator of mitochondrial calcium uptake**

(A–D) Aequorin-based, high-throughput assay of mtCa$^{2+}$ uptake was developed to select MCU-specific natural bioactives from a library of 5,571 natural food bioactive molecules. (A) Workflow and results of the screen. (B) Results of mtCa$^{2+}$ primary screen in HeLa cells stimulated with 100 µM histamine; primary hits

*(legend continued on next page)*

human skeletal muscle and dissected how its primary circulating metabolite, oleuropein-a, can stimulate mitochondrial calcium uptake at the molecular level in muscle cells. Oleuropein-a potently stimulated mt$Ca^{2+}$ uptake in primary myotubes differentiated from human skeletal muscle and stimulated with caffeine to mimic contraction (Figure 4A), without affecting cytosolic $Ca^{2+}$ elevation (Figures S4A and S4B). Similar to what was observed in HeLa cells, the primary circulating oleuropein-a metabolite was more active than the parent glycosylated molecule and the downstream metabolite hydroxytyrosol to raise mt$Ca^{2+}$ in human muscle cells (Figure 4B), prompting us to focus further cellular exploration on deglycosylated oleuropein. To confirm that oleuropein is a bona fide activator of mt$Ca^{2+}$ uptake across models, we demonstrated that it can activate mt$Ca^{2+}$ uptake using mouse muscle cells and independent sensors and calcium-release stimulation. In C2C12 myotubes (Figure S4C), oleuropein-a potently stimulated mt$Ca^{2+}$ uptake using the genetically encoded ratiometric fluorescence resonance energy transfer (FRET)-based sensor 4mtD3cpv in single cells (Figures S4C and S4D) or by stimulating calcium release with KCl (Figures S4E and S4F). We also verified that oleuropein has no effect on mitochondrial membrane potential, indicating that the increase in mt$Ca^{2+}$ was not due to alterations in the driving force for mt$Ca^{2+}$ entry (Figures S4G and S4H). Consistent with the rate-limiting role of MCU for mt$Ca^{2+}$ uptake,[32,33] adeno-associated virus (AAV)-mediated shRNA kd of MCU (MCU-kd), which strongly reduced MCU protein levels, abolished caffeine-induced mt$Ca^{2+}$ uptake (Figure 4C). Importantly, MCU-kd completely inhibited the ability of oleuropein to stimulate mt$Ca^{2+}$ uptake (Figures 4D and 4E), demonstrating that oleuropein requires the channel subunit of the MCU complex to stimulate mt$Ca^{2+}$ uptake.

Using oxygen consumption in primary human myotubes stimulated by caffeine as a model of contraction-induced mitochondrial energy metabolism, we demonstrated that oleuropein-a acutely increases mitochondrial respiration by +67% during caffeine-induced $Ca^{2+}$ mobilization and boosts functional generation of ATP via an oligomycin-sensitive coupled respiration (Figures 4F–4H). In line with the results on mt$Ca^{2+}$ (Figure 4E), kd of MCU completely prevented the effects of oleuropein-a on coupled respiration (Figures 4G and 4H), demonstrating that MCU and mt$Ca^{2+}$ are required for oleuropein-dependent mitochondrial metabolism. We next measured the effect of oleuropein-a on cell death to verify that the augmented mt$Ca^{2+}$ uptake induced by oleuropein remains physiological. Consistent with published data from literature on the safety profile of oleuropein[49,52] and the effects of MCU overexpression in skeletal muscle,[36] oleuropein and its metabolites did not affect cell death in primary human myotubes (Figure S5A).

In order to demonstrate that oleuropein can activate mt$Ca^{2+}$ uptake in fully functional muscle fibers and investigate the metabolic consequences of this activation on contractile properties, we treated isolated myofibers from mouse flexor digitorum brevis (FDB) muscle *ex vivo*. In this system, oleuropein and its metabolites also enhanced caffeine-induced mt$Ca^{2+}$ uptake (Figures 4I, 4J, S5B, and S5C) and mitochondrial respiratory capacity (Figure 4K). To determine the effect of oleuropein on skeletal muscle performance, we measured muscle strength and fatigue. Oleuropein did not show any detrimental effect on force production (Figure S6). Mitochondrial metabolism and oxidative capacity, which are boosted by oleuropein (Figures 4F, 4H, and 4K), are important to sustain muscle energy production during repeated contractions and to prevent fatigue during physical activity. Oleuropein-treated myofibers could maintain high intensity force during repeated contractions better than the untreated controls, demonstrating that oleuropein lowers fatiguability during exercise (Figure 4L). Altogether, these results demonstrate that oleuropein enhances mitochondrial energy metabolism across different models of skeletal muscle and improves the resistance to fatigue during contraction.

We then performed *in silico* docking simulations on the crystal structure of MCU subunits in order to understand how oleuropein activates the MCU complex at a molecular level. Through molecular docking and dynamics, we identified that oleuropein and oleuropein-a can bind a cleft of human *MICU1* (Figures 4M and 4N), which was also recently reported as a ligand binding pocket.[50] For the analysis of the docking, we measured the strength of the interaction (Figure 4N). The stability of conformation and the quality of the interaction indicated that both the compounds are well accommodated into the binding site. Here, we report the best conformation obtained for oleuropein-a (Figure 4M). Oleuropein and oleuropein-a were similarly oriented in the *MICU1* binding site, with the hydroxytyrosol portion of the molecule binding Glu311 of *MICU1* and the elenolic group binding both the *MICU1* N-lobe (216–220) and C-lobe (loop 441–443) (Figure S7; Video S1).

The functional relevance of the *in silico* binding was confirmed experimentally through a loss of function of *MICU1* using *MICU1*

(green), non-active molecules (gray). Results are scale-normalized with negative control at 0 (blue) and positive control with 20 μM kaempferol at 100 (red). (C) Orthogonal replication of positive hits from the primary screen using the same assay. Positive control, kaempferol 10 μM. (D) Counter-screen of cytosolic $Ca^{2+}$ to exclude the hits that modulate both mt$Ca^{2+}$ and cytosolic $Ca^{2+}$; positive control is 100 mM extracellular $Ca^{2+}$. For (A)–(D), $n$ = 1 replicate/molecule.

(E–H) Selection and validation of the positive hit oleuropein. (E) Chemical structure of the polyphenol oleuropein. (F and G) Effect of 10 μM oleuropein on mt$Ca^{2+}$ uptake in HeLa cells stimulated with 100 μM histamine, with quantification of mt$Ca^{2+}$ peak uptake from $n$ = 8 independent experiments (G). (H) Effect of 10 μM oleuropein on cytoplasmic $Ca^{2+}$ in HeLa cells stimulated with 100 μM histamine, with quantification of cytosolic $Ca^{2+}$ peak from $n$ = 7 independent experiments (H, inset).

(I) Effect of 10 μM oleuropein aglycone on MCU activity in semi-permeabilized HeLa cells evoked with 4 μM free $Ca^{2+}$, with quantification of the slope of mt$Ca^{2+}$ uptake from $n$ = 3–6 cell culture replicates/group (inset).

(J) Steady-state analysis of the binding of oleuropein to recombinant MICU1 by surface plasmon resonance. Data points and error bars represent the average and SEM of two independent replicates.

(K–N) Effect of oleuropein and its metabolites, oleuropein aglycone and hydroxytyrosol, on mt$Ca^{2+}$ uptake induced by 5 mM caffeine in C2C12-derived myotubes. Structural formula of the molecules (K) and dose-response effect of oleuropein (L), oleuropein aglycone (M), and hydroxytyrosol (N) from $n$ = 6–8 cell culture replicates per molecule.

In all bar graphs, data are presented as mean ± SEM with $^*p < 0.05$ using a two-tailed unpaired t test.

Please cite this article in press as: Gherardi et al., Mitochondrial calcium uptake declines during aging and is directly activated by oleuropein to boost energy metabolism and skeletal muscle performance, Cell Metabolism (2024), https://doi.org/10.1016/j.cmet.2024.10.021



CellPress
OPEN ACCESS

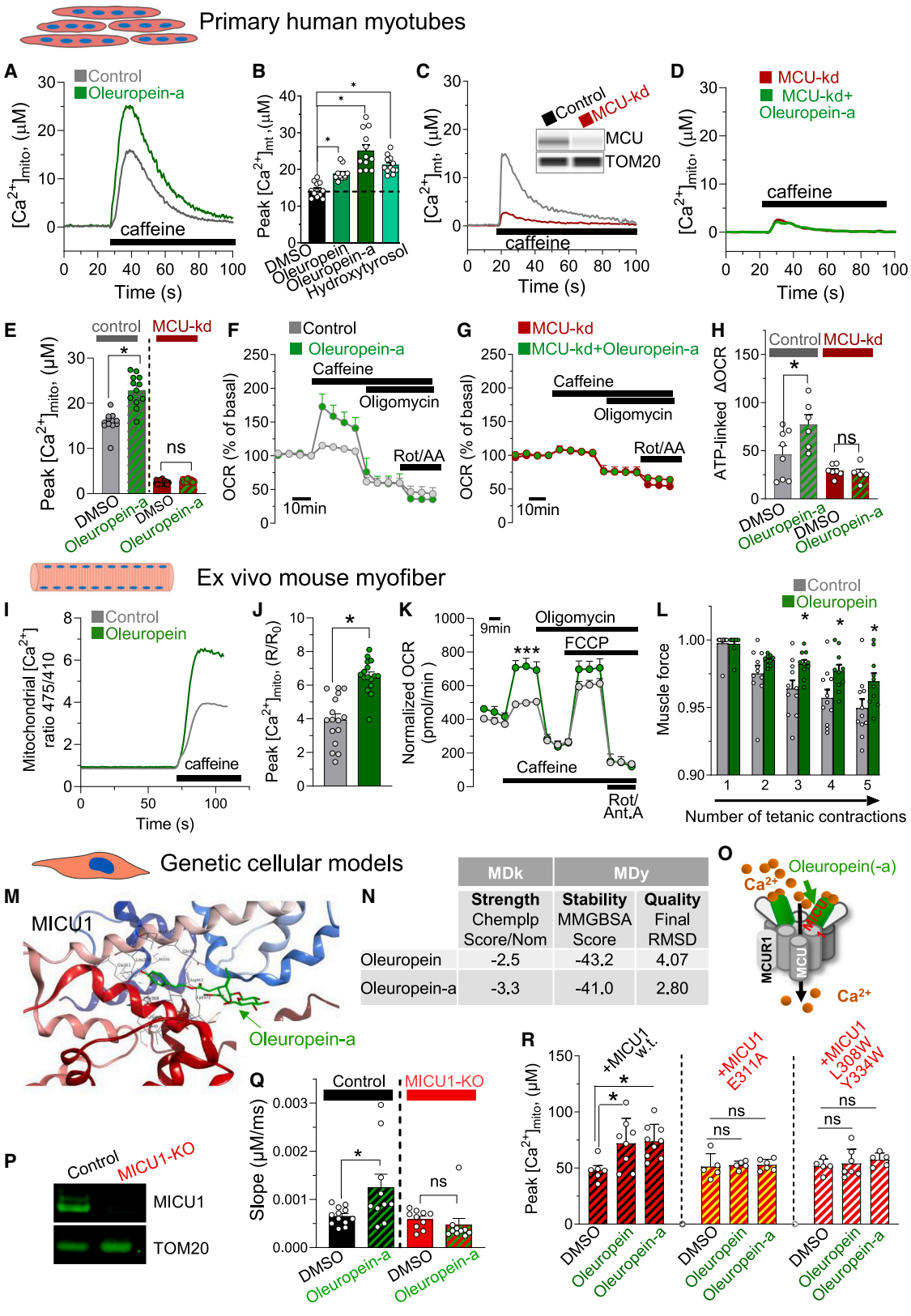


*(legend on next page)*

knockout (KO) mouse embryonic fibroblast (MEF) cells,[53] where mtCa$^{2+}$ uptake was measured in Ca$^{2+}$-stimulated semi-permeabilized cells. Similar to other models, oleuropein efficiently stimulated mtCa$^{2+}$ uptake in wild-type (WT) cells, but this response was blunted in *MICU1* KO cells (Figures 4P and 4Q). These cellular and *in silico* experiments, together with direct binding data using SPR (Figure 3J), demonstrate that oleuropein activates mtCa$^{2+}$ uptake via an MCU-dependent mechanism that relies on direct binding to MICU1 (Figure 4O). Our molecular docking analyses indicated that one of the pivotal interactions between oleuropein and *MICU1* is the hydrogen bond formation with the E311 sidechain that is deeply inserted in a sub-pocket of MICU1 occupied by the ligand. To validate the binding mode of oleuropein, we mutated E311 to an alanine residue that abolishes hydrogen bonding without creating steric hindrance in the molecular docking simulation (Figures 4M and 4N). Reintroducing WT MICU1, but not its E311A mutant, restored oleuropein-induced mtCa$^{2+}$ uptake in MICU1 KO cells (Figure 4R). To complement these results demonstrating that MICU1 E311 binding is critical for oleuropein to stimulate mtCa$^{2+}$ uptake, we performed a parallel mutagenesis approach to created steric hindrance in the predicted oleuropein binding site of MICU1. When MICU1 L308 and Y334 residues were mutated to tryptophan to occlude the binding pocket with bulky residues, the L308W/Y334W failed to restore responsiveness to oleuropein MICU1-KO cells (Figure 4R). Importantly, none of these mutants affected mtCa$^{2+}$ uptake in the absence of oleuropein (Figures 4Q and 4R). Thus, these experimental results using 2 independent mutagenesis strategies validate the *in silico* prediction of oleuropein binding to MICU1 and the requirement of the oleuropein/MICU1 interaction for mtCa$^{2+}$ uptake activation.

## Acute and chronic dietary treatments with oleuropein enhance muscle energy metabolism and performance via MCU

To determine the impact of oleuropein on energy metabolism and muscle performance in a complex physiological organism, we treated young adult mice orally via dietary administration of an olive leaf extract (OLE) standardized for high oleuropein content. A single oral dose of OLE acutely increased mtCa$^{2+}$ uptake, measured *ex vivo* in isolated myofibers (Figures 5A and 5B). In a 2- to 8-h time course after acute oral intake, OLE induced a sustained 36%–58% dephosphorylation of PDH in skeletal muscle that was already prominent after 2 h, consistent with the reported rapid peak of oleuropein and its metabolites in blood[54,55] (Figures 5C and S8A). As expected, dephosphorylation was mirrored by increased PDH activity in skeletal muscle, which was boosted by +44% after acute OLE intake (Figure 5D). Consistent with PDH activation, which is rate-limiting for pyruvate oxidation and mitochondrial oxidative metabolism, *in vivo* OLE treatment also stimulated oxygen consumption in myofibers (Figure S8B). The effects of OLE in muscle were fully maintained after chronic treatment, as dietary administration of OLE for 1 month in adult mice increased mtCa$^{2+}$ uptake (Figures 5E and 5F), decreased PDH phosphorylation (Figures 5G and S8C), increased PDH activity (Figure 5H), and stimulated oxygen consumption and mitochondrial activity (Figure 5I). Chronic OLE treatment did not affect mitochondrial DNA content (Figure S8D), indicating that changes in mitochondrial density do not contribute to higher PDH activity and mitochondrial respiration.

Muscle mass was not affected by OLE in young adult mice (Figure S8E). In contrast, OLE enhanced muscle performance by improving the resistance to fatigue in an electrically stimulated muscle force assay (Figure 5J), confirming the results obtained in isolated myofibers (Figure 4L). In addition, OLE enhanced exercise performance in a treadmill endurance test (Figure 5K). Because polyphenols can have pleiotropic effects and oleuropein has been reported to act via distinct mechanisms, including as an anti-oxidant,[56] we tested whether the effects of OLE on mitochondrial bioenergetics and muscle performance are mediated by MCU. To this end, dietary OLE was administered chronically to mice with a skeletal-muscle-specific deletion of MCU using Cre/lox recombination under control of the myosin light chain 1c promoter (skMCU$^{-/-}$ mice).[31] Unlike in WT (Figures 5I and 5K) and control (Figures 5L, 5M, and S8F), OLE had no effect on mitochondrial oxygen consumption, treadmill performance, and PDH phosphorylation in skMCU$^{-/-}$ mice (Figures 5N, 5O, and S8G). These results demonstrate

**Figure 4. Oleuropein activates mitochondrial energy metabolism in primary human myotubes and intact skeletal muscle via MICU1-dependent mtCa$^{2+}$ uptake**

(A–E) Aequorin-based mtCa$^{2+}$ uptake in control (A, B, and E) and MCU knockdown (C–E) primary human myotubes treated with 10 μM oleuropein metabolites (A, B, D, and E). (E) Caffeine (5 mM) stimulated-mtCa$^{2+}$ peak was quantified from $n$ = 12 and $n$ = 48 cell culture replicates/group for control and MCU-kd conditions, respectively.

(F–H) OCR of control (F and H) and MCU knockdown (G and H) primary human myotubes treated with 10 μM oleuropein-a. The Ca$^{2+}$-dependent mitochondrial respiratory capacity for ATP production was calculated as the OCR difference (ΔOCR) between caffeine- and oligomycin-dependent respiration in $n$ = 6–12 cell culture replicates/group (H). Caffeine, 5 mM.

(I and J) 4mtGCaMP6f-based mtCa$^{2+}$ uptake in isolated mouse FDB fibers treated with 10 μM oleuropein. 30 mM-caffeine-stimulated-mtCa$^{2+}$ peak was quantified from $n$ > 20 fibers/group.

(K) OCR of isolated FDB myofibers treated with 10 μM oleuropein. Data are normalized on mean calcein fluorescence ($n$ = 10 samples/group).

(L) *Ex vivo* fatigue of mouse EDL muscle treated with 10 μM oleuropein during repeated electrical stimulation of tetanic force; $n$ = 10 mice/group.

(M–Q) Oleuropein activates mtCa$^{2+}$ uptake by binding MICU1. (M) *In silico* docking of oleuropein-a (green) to the MICU1 crystal structure. (N) Quantification of molecular docking (MDk) and molecular dynamics (MDy) of oleuropein and oleuropein-a to MICU1. (O) Model of oleuropein-dependent activation of mtCa$^{2+}$ uptake via MICU1 binding. (P) Western blot validation of MICU1-KO in MEF cells with TOM20 as loading control. (Q) MCU activity in semi-permeabilized control and MICU1-KO MEF cells treated with 10 μM oleuropein-a, with quantification of the slope of mtCa$^{2+}$ uptake evoked with 4 μM free Ca$^{2+}$ from $n$ = 10 cellular replicates.

(R) Effect of 10 μM oleuropein and 10 μM oleuropein-a on mtCa$^{2+}$ uptake in *MICU1*-KO MEFs cells in which wild-type (*MICU1*) or site-directed mutagenized *MICU1* (*MICU1* E322A and *MICU1* L308W,Y334W) was re-introduced, as indicated. ATP stimulated-mtCa$^{2+}$ peak was quantified from $n$ > 5 samples/group.

In all bar graphs, data are presented as mean ± SEM. *$p$ < 0.05 and ns, not significant, using a one-way ANOVA (A–H) or a two-tailed unpaired t test (J–L and Q).

Please cite this article in press as: Gherardi et al., Mitochondrial calcium uptake declines during aging and is directly activated by oleuropein to boost energy metabolism and skeletal muscle performance, Cell Metabolism (2024), https://doi.org/10.1016/j.cmet.2024.10.021



CellPress
OPEN ACCESS

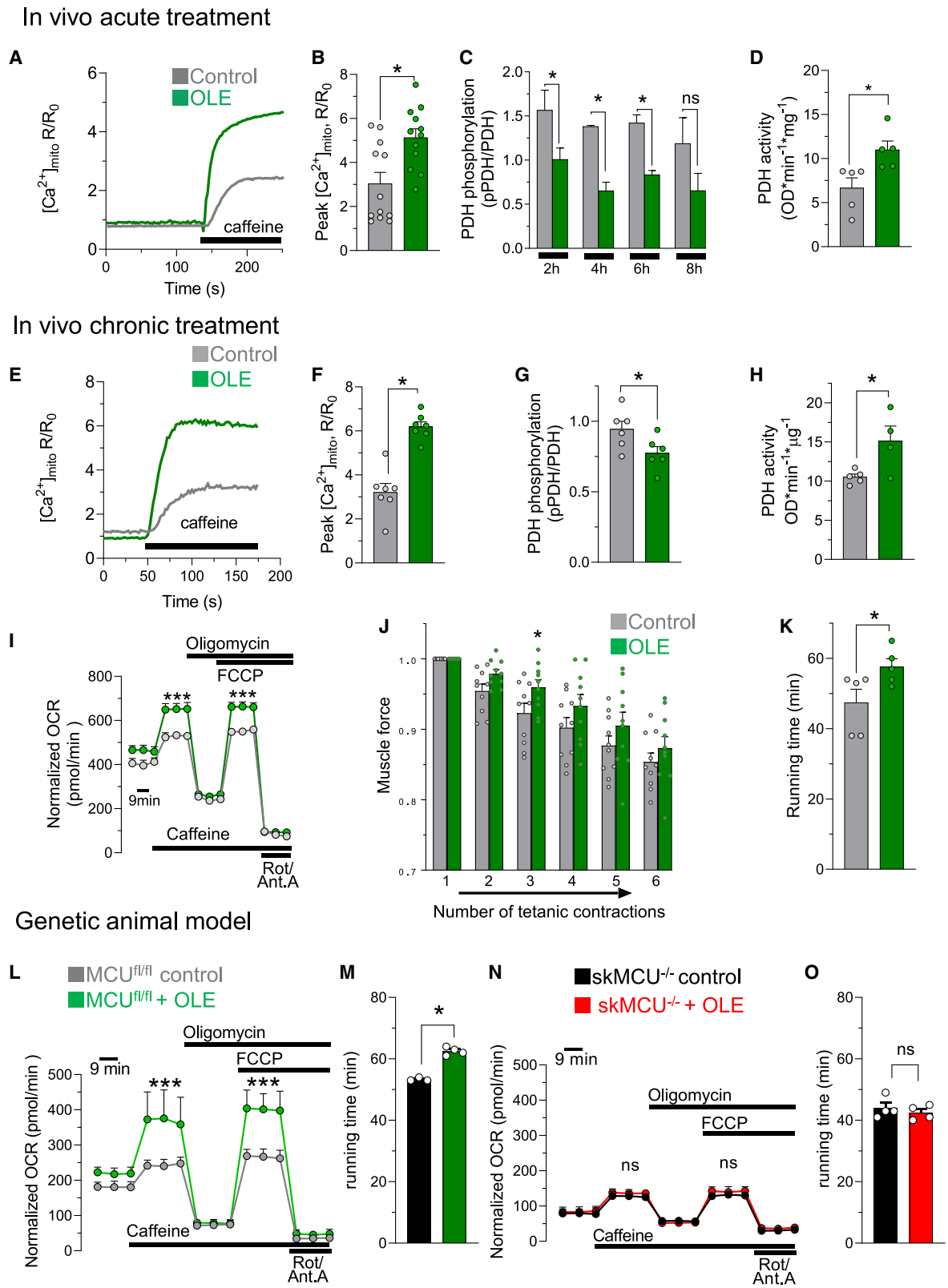


**Figure 5. Acute and chronic dietary oleuropein activates skeletal muscle energy metabolism and enhances performance *in vivo* via MCU**

(A–D) 4mtGCaMP6f-based mtCa$^{2+}$ uptake (A and B), PDH phosphorylation (C), and PDH activity (D) in skeletal muscle of young adult mice acutely receiving a single oral dose of olive leaf extract with 40% oleuropein (OLE) at 50 mg/kg or control vehicle. Representative mtCa$^{2+}$ traces (A) and quantification of mtCa$^{2+}$

*(legend continued on next page)*

that the stimulation of mitochondrial calcium uptake by OLE in healthy adults acutely and chronically activates PDH, stimulates mitochondrial respiration, and enhances exercise performance specifically via MCU.

### Oleuropein reverses the age-related decline of muscle bioenergetics and performance across species

Building on the observation that $mtCa^{2+}$ uptake and mitochondrial metabolism decline during aging and sarcopenia via a MCUR1-driven mechanism (Figures 1A–1J; Migliavacca et al.[15]), we tested whether oleuropein binding via *MICU1* could still activate $mtCa^{2+}$ uptake in aged muscle with decreased MCUR1. The effect of oleuropein on $mtCa^{2+}$ uptake was dominant over impaired muscle MCU activity caused by downregulation of *MCUR1* (Figures 1J–1L), as oleuropein-a could efficiently stimulate $mtCa^{2+}$ uptake in human primary myotubes where *MCUR1* was genetically knocked down (Figures 1K, 6A, and 6B). Oleuropein-a also reversed age-related decline of $mtCa^{2+}$ uptake in primary myotubes from aged human donors (Figures 6C and 6D). Because the decline of *MCUR1* and $mtCa^{2+}$ occurring during human aging is conserved in rodent models (Figures 2A–2G), we used complementary *in vivo* models to test whether stimulating $mtCa^{2+}$ uptake with oleuropein can reverse age-related muscle decline. In a rat model of sarcopenia with strong mitochondrial dysfunction,[57,58] chronic dietary OLE administration after the onset of sarcopenia robustly reduced PDH phosphorylation by 60% (Figures 6E–6G), indicative of enhanced activity and restored mitochondrial oxidative metabolism. Chronic dietary OLE also enhanced mitochondrial respiration of aged myofibers (Figure 6H) and restored exercise performance (Figure 6I) in a mouse aging model where mitochondrial activity and running performance decline (Figure 2H; Yanai and Endo[59]). Similar to what was observed in young mice (Figure S8D), OLE had no adaptive effect on mitochondrial mass measured via mitochondrial DNA content (Figure 6K). In addition, and distinct from young adults (Figure S8E), OLE increased muscle mass in aged mice (Figure 6J).

Taken together, these results demonstrate that oleuropein overcomes MCUR1 decline during aging to rescue MCU activity and prevent bioenergetic and functional performance impairments of aged skeletal muscle across species (Figures 6L and S9).

## DISCUSSION

Targeting mitochondria to boost bioenergetics and energy production has been an area of intense investigation over the past decade, given the major role of mitochondrial health in adaptations to lifestyle and environment and the prominent role of mitochondrial dysfunction in many chronic and genetic diseases. In the present study, we have identified the natural polyphenol oleuropein as a potent dietary molecule that directly stimulates energy production in healthy and pathological mitochondria by stimulating mitochondrial respiration and ATP production via $mtCa^{2+}$ uptake. Mechanistically, oleuropein and its deglycosylated metabolite bind to the MICU1 regulatory subunit of MCU and stimulate the uptake of $Ca^{2+}$ in mitochondria, thereby transiently increasing $mtCa^{2+}$ concentrations at physiological levels and activating dephosphorylation of PDH via the $Ca^{2+}$-dependent phosphatase PDP. Kaempferol is another natural molecule previously reported to activate $mtCa^{2+}$ uptake exclusively in cellular models.[48,51] Although it was also detected in our primary $mtCa^{2+}$ uptake screen, it failed to pass specificity for MCU as it also potentiated cytoplasmic calcium. Other mitochondrial therapeutic strategies that stabilize mitochondrial activity by indirectly targeting pathological impairments of molecular pathways and metabolic processes have translated to the clinics.[60] Elamipretide (SS-31) protects against mitochondrial dysfunction in genetic mitochondrial diseases by stabilizing the respiratory chain.[11,12] Urolithin-A is a natural postbiotic that increases muscle strength in older people by restoring youthful mitophagy.[9,61,62] Finally, $NAD^+$ precursors mitigate pathological progression in aging or genetic mitochondrial diseases by replenishing the critical metabolic cofactor $NAD^+$.[5–7,63] In contrast to these adaptive effects, activation of $mtCa^{2+}$ uptake by oleuropein is direct and occurs minutes after cellular exposure, leading to rapid activation of PDH activity and mitochondrial respiration. Importantly, oleuropein can also boost the metabolism of healthy mitochondria via a direct mechanism that acutely stimulates TCA cycle activity. Thus, oleuropein is a unique nutritional solution for mitochondrial therapeutics and a direct nutritional activator of mitochondrial bioenergetic fluxes.

Oleuropein and its metabolite hydroxytyrosol are enriched in Mediterranean diets with high olive and olive oil consumption.[56,64] Their anti-oxidant and anti-inflammatory properties have been shown to protect from cardiovascular and metabolic diseases and musculoskeletal diseases[56,65,66] and are believed to contribute to the beneficial effects of health-protective Mediterranean diets through molecular mechanisms that remain elusive. Oleuropein is the most abundant polyphenol in olive leaves,[49] which are traditionally consumed as an infusion or in extracts for health benefits in Mediterranean countries and have a history of safe human consumption. Based on this traditional knowledge and recent studies on the health benefits of

peaks (B) in 30 mM-caffeine-stimulated isolated FDB myofibers of mice acutely treated with OLE ($n$ = 12 fibers from different mice/group). PDH activity was measured in tibialis anterior muscle via PDH dephosphorylation by western blot 2–8 h after oral OLE (C; $n$ = 2 mice/group) and PDH enzymatic activity 6 h after oral OLE (D; $n$ = 5 mice/group).

(E–K) 4mtGCaMP6f-based $mtCa^{2+}$ uptake (E and F), PDH phosphorylation (G), PDH activity (H), mitochondrial respiration (I), and muscle performance (J and K) in young adult mice fed a control or OLE diet equivalent to 50 mg/kg/day for 1 month. Representative $mtCa^{2+}$ traces (E) and quantification of $mtCa^{2+}$ peaks (F) in 30 mM-caffeine-stimulated isolated FDB myofibers of mice chronically receiving OLE diet ($n$ = 7 fibers/group). PDH activity in tibialis anterior muscle measured via PDH dephosphorylation normalized to GRP75 by western blot (G) and PDH enzymatic activity (H) of mice fed for 1 month with OLE diet ($n$ = 4–6 mice/group). (I) Mitochondrial respiratory capacity measured via OCR normalized to mean calcein fluorescence in isolated FDB myofibers of mice fed for 1 month with OLE diet ($n$ = 10 samples/group). (J) *In vivo* fatigue of gastrocnemius muscle during repeated electrical stimulation of tetanic force in mice fed for 1 month with OLE diet; $n$ = 10 mice/group. (K) Exercise performance assessed in mice fed for 2 weeks with OLE diet ($n$ = 5 mice/group).

(L–O) Mitochondrial respiration after 4 weeks (L and N) and exercise performance after 2 weeks (M and O) of feeding with control or OLE diet equivalent to 50 mg/kg/day in young control ($MCU^{fl/fl}$; L and M) or skeletal-muscle-specific MCU KO ($skMCU^{-/-}$; N and O) mice ($n$ = 3–4 mice/group).

In all bar graphs, data are presented as mean ± SEM with $^*p < 0.05$ using a two-tailed unpaired t test.

Please cite this article in press as: Gherardi et al., Mitochondrial calcium uptake declines during aging and is directly activated by oleuropein to boost energy metabolism and skeletal muscle performance, Cell Metabolism (2024), https://doi.org/10.1016/j.cmet.2024.10.021



CellPress
OPEN ACCESS

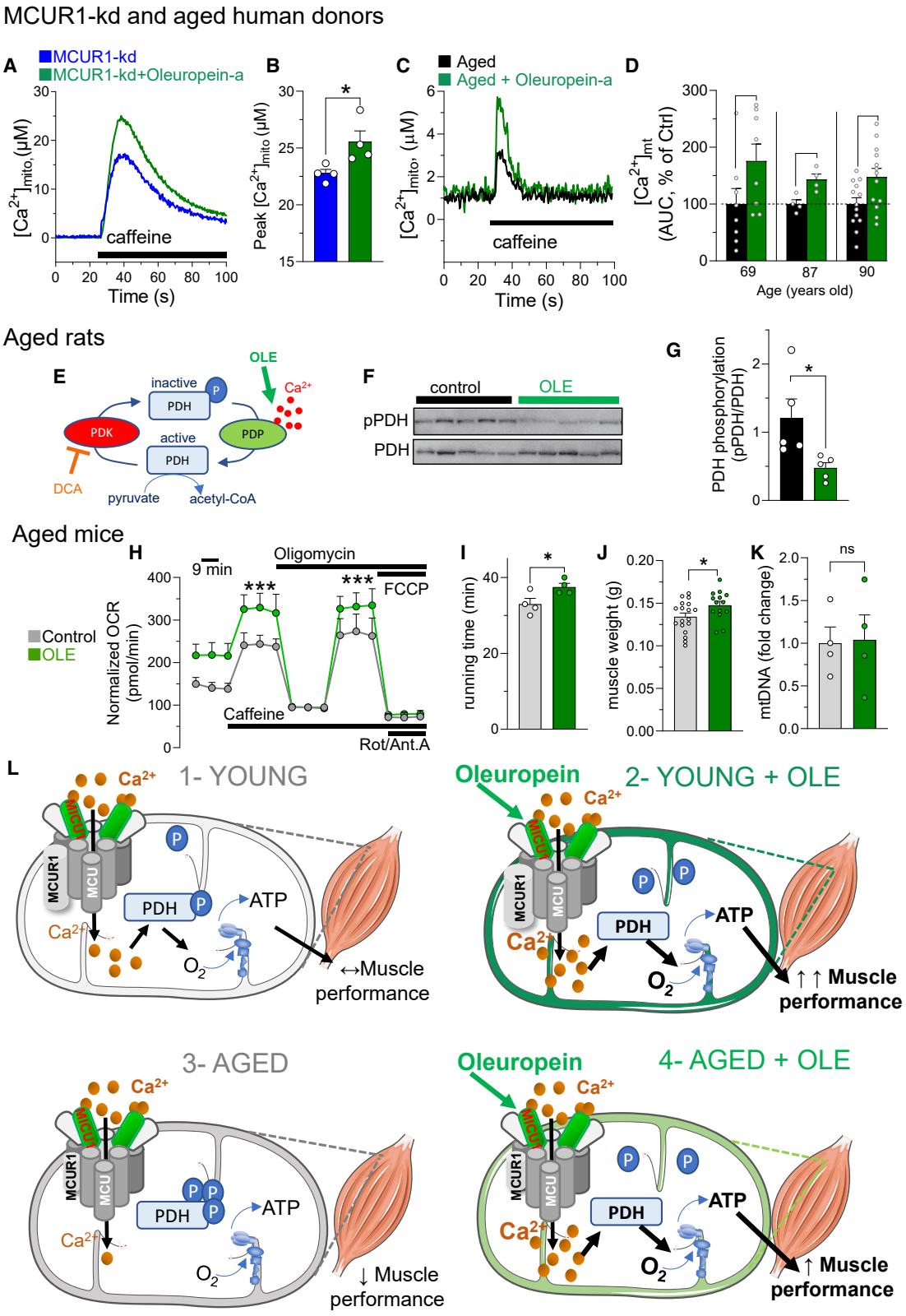


**Figure 6. Oleuropein reverses age-related decline of mtCa$^{2+}$ uptake, energy metabolism, and muscle performance across species**

(A–D) mtCa$^{2+}$ uptake in primary human myotubes with MCUR1 kd (A and B) or from aged donors (C and D) and treated with 10 μM oleuropein-a; *n* = 4 or more cellular replicates/condition.

*(legend continued on next page)*

Please cite this article in press as: Gherardi et al., Mitochondrial calcium uptake declines during aging and is directly activated by oleuropein to boost energy metabolism and skeletal muscle performance, Cell Metabolism (2024), https://doi.org/10.1016/j.cmet.2024.10.021



oleuropein,[56,65,67] OLEs with high oleuropein content have been developed for human consumption, with documented toxicological studies and clinical trials supporting the safety of oral use in humans.[49,52,66] Unlike kaempferol, oleuropein does not influence cytoplasmic $Ca^{2+}$, thereby enabling a better specificity profile that contributes to its good tolerability and safety profile. In addition, our work establishes the *in vivo* efficacy of oleuropein by demonstrating that the direct activation of $mtCa^{2+}$ uptake and mitochondrial bioenergetics by oleuropein boosts oxidative metabolism in young healthy skeletal muscle and thereby protects from muscle fatigue and stimulates endurance exercise performance. Importantly, the action of oleuropein on mitochondrial activity and muscle performance is both very fast and very specific, as KO or point mutations of the *MICU1* subunit that directly binds the molecule abrogate its action on $mtCa^{2+}$, and muscle-specific KO of *MCU* blunts its benefits on mitochondrial respiration and exercise performance.

Aging has been suggested to interfere with $mtCa^{2+}$ uptake in preclinical models,[68] and associations of MCU expression with exercise training have been reported in older people[69] without establishing whether these associations contribute to aging phenotypes. With its translational models and mechanistic experiments using genetic and pharmacological gain of function, our work establishes impaired uptake of $mtCa^{2+}$ via MCU as a hallmark of aging that causally contributes to mitochondrial dysfunction and impaired energy production and to fatigue and reduced physical performance during sarcopenia. We demonstrate that the functional capacity to take up $Ca^{2+}$ in mitochondria is altered during aging of skeletal muscle both in rodent and human models and is exacerbated by pathological progression to sarcopenia. This dysfunctional $mtCa^{2+}$ transport impairs PDH activity, mitochondrial respiration, and exercise performance. Nuclear MICU3 levels have been reported to decline in aged mice, with MICU3 overexpression partially restoring muscle decline.[70] In our study, a transcriptional downregulation of the *MCUR1* subunit of MCU directly associated with the age-related decline of $mtCa^{2+}$ uptake both in rodents and humans, whereas the expression of the structural components of the MCU complex (MCU/MCUb and MICU1/2/3) remained normal. *MCUR1* expression was low in muscle biopsies of older people with sarcopenia and mitochondrial dysfunction[15] and was positively associated with muscle mass, muscle strength, and quality of life. Although MCUR1 was initially described as a bona fide MCU regulator,[42,45] current evidence indicates that it may act as a scaffolding protein for MCU[44] and possibly other inner membrane protein complexes such as cytochrome *c* oxidase.[43] The mechanism of *MCUR1*-mediated alteration of $mtCa^{2+}$ uptake during aging is, however, direct, as *MCUR1* kd in primary human myotubes is sufficient to impair $mtCa^{2+}$ uptake and recapitulate the effect of aging. Although aging is a multi-factorial process and multiple mechanisms likely contribute to impaired $mtCa^{2+}$ uptake and mitochondrial dysfunction, our results demonstrate that the downregulation of MCUR1 is a direct causal mechanism, as genetic re-expression of *MCUR1* in aged muscle could restore defective $mtCa^{2+}$ uptake and mitochondrial respiration.

Consistent with preclinical studies where genetic modulation of $mtCa^{2+}$ and MCU in skeletal muscle regulates oxidative metabolism, mitochondrial energy production, and muscle performance in young, healthy conditions,[31,36] we demonstrate that MCU/$mtCa^{2+}$/PDH/mitochondrial oxidative phosphorylation (OxPhos) signaling in skeletal muscle also controls mitochondrial activity and muscle physiology during aging. Pharmacological activation of PDH via inhibition of PDK with DCA activates mitochondrial respiration and muscle performance and overrides reduced MCU/PDH activity during aging. Importantly, oleuropein can reverse mitochondrial and functional phenotypes of sarcopenia, as the oleuropein-mediated stimulation of $mtCa^{2+}$ uptake capacity via MICU1 is dominant over the age-related decline of MCUR1 that drives impaired $mtCa^{2+}$ uptake in aged muscle. Restoring PDH activity with oleuropein or with DCA in aged muscle is sufficient to restore mitochondrial bioenergetic potential and oxidative metabolism to improve muscle fatigue and exercise performance. Chronic oleuropein treatment also increases muscle mass in aged muscle, likely by preventing age-related muscle wasting through secondary adaptation to better performance and activity, as muscle hypertrophy was not detected in young mice or after acute treatment. Given its history of safe human use, oleuropein is therefore a promising candidate for the therapeutic management of sarcopenia and other age-related pathologies with mitochondrial dysfunction and impaired mitochondrial energy production. Its MCU-mediated mechanism of action can be complementary to the anabolic effects of protein and signaling via vitamin D, suggesting that it can be beneficial with well-accepted nutritional solutions for sarcopenia.[21,26,27]

By combining complementary cellular, animal, and clinical studies, our work establishes a causal relationship between $mtCa^{2+}$ uptake via the MCU complex, mitochondrial energy production, and muscle performance that responds to physiological, pathological, and therapeutic stimulation. The modulation of this metabolic pathway is dynamically regulated via acute nutritional signals that directly modulate metabolic fluxes and mitochondrial activity and become chronically impaired during human aging and sarcopenia. Acute consumption of the natural polyphenol oleuropein translates into optimized muscle energy coupling and ergogenic effects on performance and endurance in healthy conditions, while chronic dietary oleuropein reverses mitochondrial dysfunction and impaired muscle mass and muscle performance during sarcopenia. Given the history of safe

(E–G) PDH activation measured by dephosphorylation by western blot relative to GRP75 in gastrocnemius muscle of aged rats of 21–24 months fed with a control or OLE diet equivalent to 25 mg/kg/day for 3 months ($n$ = 5 rats/group).
(H–J) Mitochondrial respiration after 4 weeks (H), treadmill exercise performance after 2 weeks (I), and muscle weight after 4 weeks of feeding with control or OLE diet equivalent to 50 mg/kg/day in 24-month-old mice. (H) Mitochondrial respiratory capacity measured via OCR normalized to mean calcein fluorescence in isolated FDB myofibers ($n$ = 10 samples/group). (I) Exercise performance assessed in mice fed for 2 weeks with control or OLE diet ($n$ = 4 mice/group).
(K) Mitochondrial DNA content of aged mice treated with OLE, as described in (I). Data are presented as mean ± SEM of 4 muscles per condition.
(L) Model of oleuropein-dependent activation of mitochondria via MCU and protection from muscle decline during aging.
In all bar graphs, data are presented as mean ± SEM with $^*p < 0.05$ using a two-tailed unpaired t test.

human use of oleuropein and polyphenol-/olive-rich diets, our discovery opens exciting opportunities for translation to clinical trials and applications for the prevention and medical management of sarcopenia and other age-related diseases.

## Limitations of the study

Convergent evidence demonstrates that mitochondrial calcium uptake declines during aging and sarcopenia in mice and humans. Although MCUR1 expression was reduced in muscle biopsies of sarcopenic male patients from Singapore in the retrospective Multi-Ethnic Molecular determinants of Sarcopenia (MEMOSA) cohort,[15] one limitation of our work is that functional quantification of mitochondrial calcium uptake was performed in *ex vivo* primary human muscle cells but could not be performed directly in human muscle biopsies as this requires a prospective study with *ex vivo* analysis in living, dissociated myofibers. Replication of these findings and expansion across genders in different human aging cohorts, where sarcopenia may arise from different genetic and environmental origins, will be important. To this end, the Study of Muscle, Mobility and Aging (SOMMA) US cohort that analyzed muscle biopsies and mitochondrial bioenergetics in relation to muscle function, frailty, and quality of life in older men and women from the US will be of particular interest.[71] Another limitation arises from the fact that metabolic homeostasis and physio-pathological decline during aging are multi-factorial and involve crosstalk between different organs. Although our genetic and nutritional experiments demonstrated a causal role for muscle MCUR1 decline during sarcopenia and a requirement for muscle MCU for oleuropein-induced phenotypes, oleuropein may also affect other organs, and the impact on systemic metabolism, such as VO2max and substrate utilization, will deserve further investigation. Moreover, other mechanisms can contribute to impaired $mtCa^{2+}$ uptake, mitochondrial dysfunction, and, more generally, to the regulation of muscle mass and function during sarcopenia. Although oleuropein is a promising nutritional solution for the management of sarcopenia, oleuropein supplementation should be coupled to a holistic approach combining physical activity and healthy nutrition with adequate protein and vitamin D intake to overcome the multi-factorial nature of age-related muscle decline.

## RESOURCE AVAILABILITY

### Lead contact

Further information and requests for resources and reagents should be directed to and will be fulfilled by the lead contact within the limits of sample availability and ethical approvals.

### Materials availability

This study did not generate new unique reagents. Uncropped western blots and source data can be found in Data S1.

### Data and code availability

RNA sequencing data from human muscle biopsies of the Singapore sarcopenia study are available at https://www.ncbi.nlm.nih.gov/geo/query/acc.cgi?acc=GSE111016.

## ACKNOWLEDGMENTS

The authors thank Patricia Coulon for contributing to the measurements of $mtCa^{2+}$ in HSMM from old donors and Carlo Viscomi for advice on mtDNA measurements. The authors are grateful to Gyorgy Hajnoczky for sharing control and Micu1$^{-/-}$ MEFs. We deeply regret the loss of our esteemed colleague and collaborator Professor Lillycrop and honor her memory through this work. K.M.G. is a guarantor for her contribution to experiments and drafting of the manuscript. The study received internal and external funding by Société des Produits Nestlé SA. C.M. received funding from the French Muscular Dystrophy Association (22493 and 24863), the Italian Ministry of University and Research (PRIN 2022B32SCL), and the Italian Veneto Region (POR FESR). R.R. received funding from the Italian Ministry of Research (PRIN 2020R28P2E), the Italian Ministry of Health (RF-2016-02363566), the University of Padova (Stars 2017), the Italian Cariparo Foundation, the Italian Telethon Association (GGP16029), and the Italian Cancer Research Association. C.M. and R.R. received funding from the National Center for Gene Therapy and Drugs Based on RNA Technology, funded in the framework of the National Recovery and Resilience Plan (NRRP), Mission 4, Component 2, Investment 1.4, which is, in turn, funded by the European Union-Next Generation EU, project CN00000041, CUP C93C22002780006. K.M.G. is supported by the UK Medical Research Council (MC_UU_12011/4), the National Institute for Health and Care Research (NIHR Senior Investigator [NF-SI-0515-10042] and NIHR Southampton Biomedical Research Centre [NIHR203319]), and Alzheimer's Research UK (ARUK-PG2022A-008). G.G. received funding from the University of Padova (BIRD 2022). For the purpose of Open Access, the authors have applied a Creative Commons Attribution (CC BY) license to the Author Accepted Manuscript version arising from this submission.

## AUTHOR CONTRIBUTIONS

Conceptualization: R.R., J.N.F., C.M., and U.D.M.; methodology: G.G., A.W., F.B., B. Brinon, G.E.J., A.H., E.M., F.V., A.D.M., A.M., E.G., M.B., K.L., K.M.G., L.C., M.S., L.N., F.V., L.C., D.B., S.M., B. Blaauw, R.R., J.N.F., C.M., and U.D.M.; bioinformatics: E.M.; modeling: M.S. and S.M.; experimental activities: G.G., A.W., F.B., B. Brinon, F.V., E.G., M.B., A.D.M., A.H., L.N., and F.V; data analysis and interpretation: G.G., A.W., F.B., B. Brinon, G.E.J., A.H., E.M., F.V., A.D.M., E.G., K.L., K.M.G., L.C., M.S., L.N., F.V., L.C., D.B., S.M., B. Blaauw, R.R., J.N.F., C.M., and U.D.M.; writing of the manuscript: R.R., J.N.F., C.M., and U.D.M.; review and editing of the manuscript: all authors.

## DECLARATION OF INTERESTS

The authors A.W., F.B., B. Brinon, G.E.J., A.H., E.M., D.B., J.N.F., and U.D.M. are employees of Nestlé Research, which is part of the Société des Produits Nestlé SA (SPN). SPN has filed patents on the use of oleuropein for muscle and mitochondrial health. K.M.G. has received reimbursement for speaking at conferences sponsored by companies selling nutritional products and is part of an academic consortium that has received research funding from Bayer, Société des Produits Nestlé SA, BenevolentAI Bio Ltd., and Danone.

## STAR★METHODS

Detailed methods are provided in the online version of this paper and include the following:

- KEY RESOURCES TABLE
- EXPERIMENTAL MODEL AND STUDY PARTICIPANT DETAILS
  - Cell lines and primary human myotubes
  - Animals
- METHOD DETAILS
  - Human skeletal muscle transcriptomics
  - Mitochondrial $Ca^{2+}$ uptake in primary human skeletal muscle myotubes
  - Mitochondrial $Ca^{2+}$ uptake in human skeletal muscle myotubes from healthy and sarcopenic donors
  - High throughput screening of mitochondrial $Ca^{2+}$
  - Mitochondrial $Ca^{2+}$ uptake in C2C12 cells and Mouse Embryonic Fibroblasts (MEFs)
  - Mitochondrial $Ca^{2+}$ uptake in semi-permeabilized HeLa cells
  - MICU1 protein expression and purification, and determination of Oleuropein binding by Surface Plasmon Resonance (SPR)
  - Mitochondrial respiration in primary human myotubes

## SUPPLEMENTAL INFORMATION

Supplemental information can be found online at https://doi.org/10.1016/j.cmet.2024.10.021.

Received: April 7, 2023
Revised: July 24, 2024
Accepted: October 23, 2024
Published: November 25, 2024

## REFERENCES


1. López-Otín, C., Blasco, M.A., Partridge, L., Serrano, M., and Kroemer, G. (2023). Hallmarks of aging: An expanding universe. Cell *186*, 243–278. https://doi.org/10.1016/j.cell.2022.11.001.
2. Sun, N., Youle, R.J., and Finkel, T. (2016). The Mitochondrial Basis of Aging. Mol. Cell *61*, 654–666. https://doi.org/10.1016/j.molcel.2016.01.028.
3. Kulkarni, A.S., Gubbi, S., and Barzilai, N. (2020). Benefits of Metformin in Attenuating the Hallmarks of Aging. Cell Metab. *32*, 15–30. https://doi.org/10.1016/j.cmet.2020.04.001.
4. Covarrubias, A.J., Perrone, R., Grozio, A., and Verdin, E. (2021). $NAD^+$ metabolism and its roles in cellular processes during ageing. Nat. Rev. Mol. Cell Biol. *22*, 119–141. https://doi.org/10.1038/s41580-020-00313-x.
5. Lapatto, H.A.K., Kuusela, M., Heikkinen, A., Muniandy, M., van der Kolk, B.W., Gopalakrishnan, S., Pöllänen, N., Sandvik, M., Schmidt, M.S., Heinonen, S., et al. (2023). Nicotinamide riboside improves muscle mitochondrial biogenesis, satellite cell differentiation, and gut microbiota in a twin study. Sci. Adv. *9*, eadd5163. https://doi.org/10.1126/sciadv.add5163.
6. Martens, C.R., Denman, B.A., Mazzo, M.R., Armstrong, M.L., Reisdorph, N., McQueen, M.B., Chonchol, M., and Seals, D.R. (2018). Chronic nicotinamide riboside supplementation is well-tolerated and elevates $NAD^+$ in healthy middle-aged and older adults. Nat. Commun. *9*, 1286. https://doi.org/10.1038/s41467-018-03421-7.
7. Yoshino, M., Yoshino, J., Kayser, B.D., Patti, G.J., Franczyk, M.P., Mills, K.F., Sindelar, M., Pietka, T., Patterson, B.W., Imai, S.I., et al. (2021). Nicotinamide mononucleotide increases muscle insulin sensitivity in prediabetic women. Science *372*, 1224–1229. https://doi.org/10.1126/science.abe9985.
8. Ryu, D., Mouchiroud, L., Andreux, P.A., Katsyuba, E., Moullan, N., Nicolet-Dit-Félix, A.A., Williams, E.G., Jha, P., Lo Sasso, G., Huzard, D., et al. (2016). Urolithin A induces mitophagy and prolongs lifespan in C. elegans and increases muscle function in rodents. Nat. Med. *22*, 879–888. https://doi.org/10.1038/nm.4132.
9. Andreux, P.A., Blanco-Bose, W., Ryu, D., Burdet, F., Ibberson, M., Aebischer, P., Auwerx, J., Singh, A., and Rinsch, C. (2019). The mitophagy activator urolithin A is safe and induces a molecular signature of improved mitochondrial and cellular health in humans. Nat. Metab. *1*, 595–603. https://doi.org/10.1038/s42255-019-0073-4.
10. Eisenberg, T., Abdellatif, M., Schroeder, S., Primessnig, U., Stekovic, S., Pendl, T., Harger, A., Schipke, J., Zimmermann, A., Schmidt, A., et al. (2016). Cardioprotection and lifespan extension by the natural polyamine spermidine. Nat. Med. *22*, 1428–1438. https://doi.org/10.1038/nm.4222.
11. Chavez, J.D., Tang, X., Campbell, M.D., Reyes, G., Kramer, P.A., Stuppard, R., Keller, A., Zhang, H., Rabinovitch, P.S., Marcinek, D.J., et al. (2020). Mitochondrial protein interaction landscape of SS-31. Proc. Natl. Acad. Sci. USA *117*, 15363–15373. https://doi.org/10.1073/pnas.2002250117.
12. Karaa, A., Haas, R., Goldstein, A., Vockley, J., Weaver, W.D., and Cohen, B.H. (2018). Randomized dose-escalation trial of elamipretide in adults with primary mitochondrial myopathy. Neurology *90*, e1212–e1221. https://doi.org/10.1212/WNL.0000000000005255.
13. Hargreaves, M., and Spriet, L.L. (2020). Skeletal muscle energy metabolism during exercise. Nat. Metab. *2*, 817–828. https://doi.org/10.1038/s42255-020-0251-4.
14. Menshikova, E.V., Ritov, V.B., Fairfull, L., Ferrell, R.E., Kelley, D.E., and Goodpaster, B.H. (2006). Effects of exercise on mitochondrial content and function in aging human skeletal muscle. J. Gerontol. A Biol. Sci. Med. Sci. *61*, 534–540. https://doi.org/10.1093/gerona/61.6.534.
15. Migliavacca, E., Tay, S.K.H., Patel, H.P., Sonntag, T., Civiletto, G., McFarlane, C., Forrester, T., Barton, S.J., Leow, M.K., Antoun, E., et al. (2019). Mitochondrial oxidative capacity and $NAD^+$ biosynthesis are reduced in human sarcopenia across ethnicities. Nat. Commun. *10*, 5808. https://doi.org/10.1038/s41467-019-13694-1.
16. Hood, D.A., Memme, J.M., Oliveira, A.N., and Triolo, M. (2019). Maintenance of Skeletal Muscle Mitochondria in Health, Exercise, and Aging. Annu. Rev. Physiol. *81*, 19–41. https://doi.org/10.1146/annurev-physiol-020518-114310.
17. Short, K.R., Bigelow, M.L., Kahl, J., Singh, R., Coenen-Schimke, J., Raghavakaimal, S., and Nair, K.S. (2005). Decline in skeletal muscle mitochondrial function with aging in humans. Proc. Natl. Acad. Sci. USA *102*, 5618–5623. https://doi.org/10.1073/pnas.0501559102.
18. Petersen, K.F., Befroy, D., Dufour, S., Dziura, J., Ariyan, C., Rothman, D.L., DiPietro, L., Cline, G.W., and Shulman, G.I. (2003). Mitochondrial dysfunction in the elderly: possible role in insulin resistance. Science *300*, 1140–1142. https://doi.org/10.1126/science.1082889.
19. Zane, A.C., Reiter, D.A., Shardell, M., Cameron, D., Simonsick, E.M., Fishbein, K.W., Studenski, S.A., Spencer, R.G., and Ferrucci, L. (2017). Muscle strength mediates the relationship between mitochondrial energetics and walking performance. Aging Cell *16*, 461–468. https://doi.org/10.1111/acel.12568.
20. Andreux, P.A., van Diemen, M.P.J., Heezen, M.R., Auwerx, J., Rinsch, C., Groeneveld, G.J., and Singh, A. (2018). Mitochondrial function is impaired in the skeletal muscle of pre-frail elderly. Sci. Rep. *8*, 8548. https://doi.org/10.1038/s41598-018-26944-x.
21. Cruz-Jentoft, A.J., Dawson Hughes, B., Scott, D., Sanders, K.M., and Rizzoli, R. (2020). Nutritional strategies for maintaining muscle mass and strength from middle age to later life: A narrative review. Maturitas *132*, 57–64. https://doi.org/10.1016/j.maturitas.2019.11.007.
22. Robinson, S.M., Reginster, J.Y., Rizzoli, R., Shaw, S.C., Kanis, J.A., Bautmans, I., Bischoff-Ferrari, H., Bruyère, O., Cesari, M., Dawson-Hughes, B., et al. (2018). Does nutrition play a role in the prevention and management of sarcopenia? Clin. Nutr. *37*, 1121–1132. https://doi.org/10.1016/j.clnu.2017.08.016.
23. Cartee, G.D., Hepple, R.T., Bamman, M.M., and Zierath, J.R. (2016). Exercise Promotes Healthy Aging of Skeletal Muscle. Cell Metab. *23*, 1034–1047. https://doi.org/10.1016/j.cmet.2016.05.007.
24. Bernabei, R., Landi, F., Calvani, R., Cesari, M., Del Signore, S., Anker, S.D., Bejuit, R., Bordes, P., Cherubini, A., Cruz-Jentoft, A.J., et al. (2022). Multicomponent intervention to prevent mobility disability in frail older adults: randomised controlled trial (SPRINTT project). BMJ *377*, e068788. https://doi.org/10.1136/bmj-2021-068788.

25. Pahor, M., Guralnik, J.M., Ambrosius, W.T., Blair, S., Bonds, D.E., Church, T.S., Espeland, M.A., Fielding, R.A., Gill, T.M., Groessl, E.J., et al. (2014). Effect of structured physical activity on prevention of major mobility disability in older adults: the LIFE study randomized clinical trial. JAMA *311*, 2387–2396. https://doi.org/10.1001/jama.2014.5616.

26. Deutz, N.E.P., Bauer, J.M., Barazzoni, R., Biolo, G., Boirie, Y., Bosy-Westphal, A., Cederholm, T., Cruz-Jentoft, A., Krznariç, Z., Nair, K.S., et al. (2014). Protein intake and exercise for optimal muscle function with aging: recommendations from the ESPEN Expert Group. Clin. Nutr. *33*, 929–936. https://doi.org/10.1016/j.clnu.2014.04.007.

27. Morley, J.E., Argiles, J.M., Evans, W.J., Bhasin, S., Cella, D., Deutz, N.E.P., Doehner, W., Fearon, K.C.H., Ferrucci, L., Hellerstein, M.K., et al. (2010). Nutritional recommendations for the management of sarcopenia. J. Am. Med. Dir. Assoc. *11*, 391–396. https://doi.org/10.1016/j.jamda.2010.04.014.

28. Trichopoulou, A., Costacou, T., Bamia, C., and Trichopoulos, D. (2003). Adherence to a Mediterranean diet and survival in a Greek population. N. Engl. J. Med. *348*, 2599–2608. https://doi.org/10.1056/NEJMoa025039.

29. Trichopoulou, A., Kouris-Blazos, A., Wahlqvist, M.L., Gnardellis, C., Lagiou, P., Polychronopoulos, E., Vassilakou, T., Lipworth, L., and Trichopoulos, D. (1995). Diet and overall survival in elderly people. BMJ *311*, 1457–1460. https://doi.org/10.1136/bmj.311.7018.1457.

30. Rizzuto, R., De Stefani, D., Raffaello, A., and Mammucari, C. (2012). Mitochondria as sensors and regulators of calcium signalling. Nat. Rev. Mol. Cell Biol. *13*, 566–578. https://doi.org/10.1038/nrm3412.

31. Gherardi, G., Nogara, L., Ciciliot, S., Fadini, G.P., Blaauw, B., Braghetta, P., Bonaldo, P., De Stefani, D., Rizzuto, R., and Mammucari, C. (2019). Loss of mitochondrial calcium uniporter rewires skeletal muscle metabolism and substrate preference. Cell Death Differ. *26*, 362–381. https://doi.org/10.1038/s41418-018-0191-7.

32. Baughman, J.M., Perocchi, F., Girgis, H.S., Plovanich, M., Belcher-Timme, C.A., Sancak, Y., Bao, X.R., Strittmatter, L., Goldberger, O., Bogorad, R.L., et al. (2011). Integrative genomics identifies MCU as an essential component of the mitochondrial calcium uniporter. Nature *476*, 341–345. https://doi.org/10.1038/nature10234.

33. De Stefani, D., Raffaello, A., Teardo, E., Szabò, I., and Rizzuto, R. (2011). A forty-kilodalton protein of the inner membrane is the mitochondrial calcium uniporter. Nature *476*, 336–340. https://doi.org/10.1038/nature10230.

34. Gherardi, G., Monticelli, H., Rizzuto, R., and Mammucari, C. (2020). The Mitochondrial $Ca^{2+}$ Uptake and the Fine-Tuning of Aerobic Metabolism. Front. Physiol. *11*, 554904. https://doi.org/10.3389/fphys.2020.554904.

35. Zanou, N., Dridi, H., Reiken, S., Imamura de Lima, T., Donnelly, C., De Marchi, U., Ferrini, M., Vidal, J., Sittenfeld, L., Feige, J.N., et al. (2021). Acute RyR1 $Ca^{2+}$ leak enhances NADH-linked mitochondrial respiratory capacity. Nat. Commun. *12*, 7219. https://doi.org/10.1038/s41467-021-27422-1.

36. Mammucari, C., Gherardi, G., Zamparo, I., Raffaello, A., Boncompagni, S., Chemello, F., Cagnin, S., Braga, A., Zanin, S., Pallafacchina, G., et al. (2015). The mitochondrial calcium uniporter controls skeletal muscle trophism in vivo. Cell Rep. *10*, 1269–1279. https://doi.org/10.1016/j.celrep.2015.01.056.

37. Debattisti, V., Horn, A., Singh, R., Seifert, E.L., Hogarth, M.W., Mazala, D.A., Huang, K.T., Horvath, R., Jaiswal, J.K., and Hajnóczky, G. (2019). Dysregulation of Mitochondrial $Ca^{2+}$ Uptake and Sarcolemma Repair Underlie Muscle Weakness and Wasting in Patients and Mice Lacking MICU1. Cell Rep. *29*, 1274–1286.e6. https://doi.org/10.1016/j.celrep.2019.09.063.

38. Garbincius, J.F., and Elrod, J.W. (2022). Mitochondrial calcium exchange in physiology and disease. Physiol. Rev. *102*, 893–992. https://doi.org/10.1152/physrev.00041.2020.

39. Logan, C.V., Szabadkai, G., Sharpe, J.A., Parry, D.A., Torelli, S., Childs, A.M., Kriek, M., Phadke, R., Johnson, C.A., Roberts, N.Y., et al. (2014). Loss-of-function mutations in MICU1 cause a brain and muscle disorder linked to primary alterations in mitochondrial calcium signaling. Nat. Genet. *46*, 188–193. https://doi.org/10.1038/ng.2851.

40. Lewis-Smith, D., Kamer, K.J., Griffin, H., Childs, A.M., Pysden, K., Titov, D., Duff, J., Pyle, A., Taylor, R.W., Yu-Wai-Man, P., et al. (2016). Homozygous deletion in MICU1 presenting with fatigue and lethargy in childhood. Neurol. Genet. *2*, e59. https://doi.org/10.1212/NXG.0000000000000059.

41. Chaudhuri, D., Artiga, D.J., Abiria, S.A., and Clapham, D.E. (2016). Mitochondrial calcium uniporter regulator 1 (MCUR1) regulates the calcium threshold for the mitochondrial permeability transition. Proc. Natl. Acad. Sci. USA *113*, E1872–E1880. https://doi.org/10.1073/pnas.1602264113.

42. Mallilankaraman, K., Cárdenas, C., Doonan, P.J., Chandramoorthy, H.C., Irrinki, K.M., Golenár, T., Csordás, G., Madireddi, P., Yang, J., Müller, M., et al. (2012). MCUR1 is an essential component of mitochondrial Ca2+ uptake that regulates cellular metabolism. Nat. Cell Biol. *14*, 1336–1343. https://doi.org/10.1038/ncb2622.

43. Paupe, V., Prudent, J., Dassa, E.P., Rendon, O.Z., and Shoubridge, E.A. (2015). CCDC90A (MCUR1) is a cytochrome c oxidase assembly factor and not a regulator of the mitochondrial calcium uniporter. Cell Metab. *21*, 109–116. https://doi.org/10.1016/j.cmet.2014.12.004.

44. Tomar, D., Dong, Z., Shanmughapriya, S., Koch, D.A., Thomas, T., Hoffman, N.E., Timbalia, S.A., Goldman, S.J., Breves, S.L., Corbally, D.P., et al. (2016). MCUR1 Is a Scaffold Factor for the MCU Complex Function and Promotes Mitochondrial Bioenergetics. Cell Rep. *15*, 1673–1685. https://doi.org/10.1016/j.celrep.2016.04.050.

45. Vais, H., Tanis, J.E., Müller, M., Payne, R., Mallilankaraman, K., and Foskett, J.K. (2015). MCUR1, CCDC90A, Is a Regulator of the Mitochondrial Calcium Uniporter. Cell Metab. *22*, 533–535. https://doi.org/10.1016/j.cmet.2015.09.015.

46. Weisleder, N., Brotto, M., Komazaki, S., Pan, Z., Zhao, X., Nosek, T., Parness, J., Takeshima, H., and Ma, J. (2006). Muscle aging is associated with compromised Ca2+ spark signaling and segregated intracellular Ca2+ release. J. Cell Biol. *174*, 639–645. https://doi.org/10.1083/jcb.200604166.

47. Palamiuc, L., Schlagowski, A., Ngo, S.T., Vernay, A., Dirrig-Grosch, S., Henriques, A., Boutillier, A.L., Zoll, J., Echaniz-Laguna, A., Loeffler, J.P., et al. (2015). A metabolic switch toward lipid use in glycolytic muscle is an early pathologic event in a mouse model of amyotrophic lateral sclerosis. EMBO Mol. Med. *7*, 526–546. https://doi.org/10.15252/emmm.201404433.

48. Montero, M., Lobatón, C.D., Hernández-Sanmiguel, E., Santodomingo, J., Vay, L., Moreno, A., and Alvarez, J. (2004). Direct activation of the mitochondrial calcium uniporter by natural plant flavonoids. Biochem. J. *384*, 19–24. https://doi.org/10.1042/BJ20040990.

49. Clewell, A.E., Béres, E., Vértesi, A., Glávits, R., Hirka, G., Endres, J.R., Murbach, T.S., and Szakonyiné, I.P. (2016). A Comprehensive Toxicological Safety Assessment of an Extract of Olea Europaea L. Leaves (Bonolive™). Int. J. Toxicol. *35*, 208–221. https://doi.org/10.1177/1091581815619764.

50. Di Marco, G., Vallese, F., Jourde, B., Bergsdorf, C., Sturlese, M., De Mario, A., Techer-Etienne, V., Haasen, D., Oberhauser, B., Schleeger, S., et al. (2020). A High-Throughput Screening Identifies MICU1 Targeting Compounds. Cell Rep. *30*, 2321–2331.e6. https://doi.org/10.1016/j.celrep.2020.01.081.

51. Rodríguez-Prados, M., Huang, K.T., Márta, K., Paillard, M., Csordás, G., Joseph, S.K., and Hajnóczky, G. (2023). MICU1 controls the sensitivity of the mitochondrial $Ca^{2+}$ uniporter to activators and inhibitors. Cell Chem. Biol. *30*, 606–617.e4. e604. https://doi.org/10.1016/j.chembiol.2023.05.002.

52. Guex, C.G., Reginato, F.Z., Figueredo, K.C., da Silva, A.R.H.D., Pires, F.B., Jesus, R.D.S., Lhamas, C.L., Lopes, G.H.H., and Bauermann, L.F. (2018). Safety assessment of ethanolic extract of Olea europaea L. leaves after acute and subacute administration to Wistar rats. Regul. Toxicol. Pharmacol. *95*, 395–399. https://doi.org/10.1016/j.yrtph.2018.04.013.

53. Antony, A.N., Paillard, M., Moffat, C., Juskeviciute, E., Correnti, J., Bolon, B., Rubin, E., Csordás, G., Seifert, E.L., Hoek, J.B., et al. (2016). MICU1 regulation of mitochondrial Ca(2+) uptake dictates survival and tissue regeneration. Nat. Commun. *7*, 10955. https://doi.org/10.1038/ncomms10955.

54. García-Villalba, R., Larrosa, M., Possemiers, S., Tomás-Barberán, F.A., and Espín, J.C. (2014). Bioavailability of phenolics from an oleuropein-rich olive (Olea europaea) leaf extract and its acute effect on plasma antioxidant status: comparison between pre- and postmenopausal women. Eur. J. Nutr. *53*, 1015–1027. https://doi.org/10.1007/s00394-013-0604-9.

55. Polia, F., Horcajada, M.N., Poquet, L., Tomás-Barberán, F.A., and García-Villalba, R. (2022). A novel combined analytical UV and MS approach for the quantification of oleuropein metabolites in human biological samples when authentic standards are not available. J. Chromatogr. B Analyt. Technol. Biomed. Life Sci. *1210*, 123457. https://doi.org/10.1016/j.jchromb.2022.123457.

56. Bulotta, S., Celano, M., Lepore, S.M., Montalcini, T., Pujia, A., and Russo, D. (2014). Beneficial effects of the olive oil phenolic components oleuropein and hydroxytyrosol: focus on protection against cardiovascular and metabolic diseases. J. Transl. Med. *12*, 219. https://doi.org/10.1186/s12967-014-0219-9.

57. Ibebunjo, C., Chick, J.M., Kendall, T., Eash, J.K., Li, C., Zhang, Y., Vickers, C., Wu, Z., Clarke, B.A., Shi, J., et al. (2013). Genomic and proteomic profiling reveals reduced mitochondrial function and disruption of the neuromuscular junction driving rat sarcopenia. Mol. Cell. Biol. *33*, 194–212. https://doi.org/10.1128/MCB.01036-12.

58. Pannérec, A., Springer, M., Migliavacca, E., Ireland, A., Piasecki, M., Karaz, S., Jacot, G., Métairon, S., Danenberg, E., Raymond, F., et al. (2016). A robust neuromuscular system protects rat and human skeletal muscle from sarcopenia. Aging (Albany, NY) *8*, 712–729. https://doi.org/10.18632/aging.100926.

59. Yanai, S., and Endo, S. (2021). Functional Aging in Male C57BL/6J Mice Across the Life-Span: A Systematic Behavioral Analysis of Motor, Emotional, and Memory Function to Define an Aging Phenotype. Front. Aging Neurosci. *13*, 697621. https://doi.org/10.3389/fnagi.2021.697621.

60. Singh, A., Faccenda, D., and Campanella, M. (2021). Pharmacological advances in mitochondrial therapy. EBiomedicine *65*, 103244. https://doi.org/10.1016/j.ebiom.2021.103244.

61. Liu, S., D'Amico, D., Shankland, E., Bhayana, S., Garcia, J.M., Aebischer, P., Rinsch, C., Singh, A., and Marcinek, D.J. (2022). Effect of Urolithin A Supplementation on Muscle Endurance and Mitochondrial Health in Older Adults: A Randomized Clinical Trial. JAMA Netw. Open *5*, e2144279. https://doi.org/10.1001/jamanetworkopen.2021.44279.

62. Singh, A., D'Amico, D., Andreux, P.A., Fouassier, A.M., Blanco-Bose, W., Evans, M., Aebischer, P., Auwerx, J., and Rinsch, C. (2022). Urolithin A improves muscle strength, exercise performance, and biomarkers of mitochondrial health in a randomized trial in middle-aged adults. Cell Rep. Med. *3*, 100633. https://doi.org/10.1016/j.xcrm.2022.100633.

63. Pirinen, E., Auranen, M., Khan, N.A., Brilhante, V., Urho, N., Pessia, A., Hakkarainen, A., Kuula, J., Heinonen, U., Schmidt, M.S., et al. (2020). Niacin Cures Systemic $NAD^+$ Deficiency and Improves Muscle Performance in Adult-Onset Mitochondrial Myopathy. Cell Metab. *31*, 1078–1090.e5. https://doi.org/10.1016/j.cmet.2020.04.008.

64. Omar, S.H. (2010). Oleuropein in olive and its pharmacological effects. Sci. Pharm. *78*, 133–154. https://doi.org/10.3797/scipharm.0912-18.

65. Barbaro, B., Toietta, G., Maggio, R., Arciello, M., Tarocchi, M., Galli, A., and Balsano, C. (2014). Effects of the olive-derived polyphenol oleuropein on human health. Int. J. Mol. Sci. *15*, 18508–18524. https://doi.org/10.3390/ijms151018508.

66. Horcajada, M.N., Beaumont, M., Sauvageot, N., Poquet, L., Saboundjian, M., Costes, B., Verdonk, P., Brands, G., Brasseur, J., Urbin-Choffray, D., et al. (2022). An oleuropein-based dietary supplement may improve joint functional capacity in older people with high knee joint pain: findings from a multicentre-RCT and post hoc analysis. Ther. Adv. Musculoskelet. Dis. *14*, 1759720X211070205. https://doi.org/10.1177/1759720X211070205.

67. Nasrallah, H., Aissa, I., Slim, C., Boujbiha, M.A., Zaouali, M.A., Bejaoui, M., Wilke, V., Ben Jannet, H., Mosbah, H., and Ben Abdennebi, H. (2020). Effect of oleuropein on oxidative stress, inflammation and apoptosis induced by ischemia-reperfusion injury in rat kidney. Life Sci. *255*, 117833. https://doi.org/10.1016/j.lfs.2020.117833.

68. Pietrangelo, L., D'Incecco, A., Ainbinder, A., Michelucci, A., Kern, H., Dirksen, R.T., Boncompagni, S., and Protasi, F. (2015). Age-dependent uncoupling of mitochondria from $Ca^{2+}$ release units in skeletal muscle. Oncotarget *6*, 35358–35371. https://doi.org/10.18632/oncotarget.6139.

69. Zampieri, S., Mammucari, C., Romanello, V., Barberi, L., Pietrangelo, L., Fusella, A., Mosole, S., Gherardi, G., Höfer, C., Löfler, S., et al. (2016). Physical exercise in aging human skeletal muscle increases mitochondrial calcium uniporter expression levels and affects mitochondria dynamics. Physiol. Rep. *4*, 4. https://doi.org/10.14814/phy2.13005.

70. Yang, Y.F., Yang, W., Liao, Z.Y., Wu, Y.X., Fan, Z., Guo, A., Yu, J., Chen, Q.N., Wu, J.H., Zhou, J., et al. (2021). MICU3 regulates mitochondrial $Ca^{2+}$-dependent antioxidant response in skeletal muscle aging. Cell Death Dis. *12*, 1115. https://doi.org/10.1038/s41419-021-04400-5.

71. Cummings, S.R., Coen, P.M., and Ferrucci, L. (2024). The cellular bases of mobility from the Study of Muscle, Mobility and Aging (SOMMA). Aging Cell *23*, e14129. https://doi.org/10.1111/acel.14129.

72. Robinson, M.D., McCarthy, D.J., and Smyth, G.K. (2010). edgeR: a Bioconductor package for differential expression analysis of digital gene expression data. Bioinformatics *26*, 139–140. https://doi.org/10.1093/bioinformatics/btp616.

73. Liu, R., Holik, A.Z., Su, S., Jansz, N., Chen, K., Leong, H.S., Blewitt, M.E., Asselin-Labat, M.L., Smyth, G.K., and Ritchie, M.E. (2015). Why weight? Modelling sample and observational level variability improves power in RNA-seq analyses. Nucleic Acids Res. *43*, e97. https://doi.org/10.1093/nar/gkv412.

74. Antoun, E., Garratt, E.S., Taddei, A., Burton, M.A., Barton, S.J., Titcombe, P., Westbury, L.D., Baczynska, A., Migliavacca, E., Feige, J.N., et al. (2022). Epigenome-wide association study of sarcopenia: findings from the Hertfordshire Sarcopenia Study (HSS). J. Cachexia Sarcopenia Muscle *13*, 240–253. https://doi.org/10.1002/jcsm.12876.

75. Pinton, P., Rimessi, A., Romagnoli, A., Prandini, A., and Rizzuto, R. (2007). Biosensors for the detection of calcium and pH. Methods Cell Biol. *80*, 297–325. https://doi.org/10.1016/S0091-679X(06)80015-4.

76. Rizzuto, R., Simpson, A.W., Brini, M., and Pozzan, T. (1992). Rapid changes of mitochondrial Ca2+ revealed by specifically targeted recombinant aequorin. Nature *358*, 325–327. https://doi.org/10.1038/358325a0.

77. Brini, M., Marsault, R., Bastianutto, C., Alvarez, J., Pozzan, T., and Rizzuto, R. (1995). Transfected aequorin in the measurement of cytosolic Ca2+ concentration ([Ca2+]c). A critical evaluation. J. Biol. Chem. *270*, 9896–9903. https://doi.org/10.1074/jbc.270.17.9896.

78. Yannai, S. (2012). Dictionary of Food Compounds with CD-ROM (CRC Press). https://doi.org/10.1201/b12964.

79. Tosatto, A., Rizzuto, R., and Mammucari, C. (2017). $Ca^{2+}$ Measurements in Mammalian Cells with Aequorin-based Probes. Bio Protoc. *7*, 7. https://doi.org/10.21769/BioProtoc.2155.

80. Wang, L., Yang, X., Li, S., Wang, Z., Liu, Y., Feng, J., Zhu, Y., and Shen, Y. (2014). Structural and mechanistic insights into MICU1 regulation of mitochondrial calcium uptake. EMBO J. *33*, 594–604. https://doi.org/10.1002/embj.201386523.

81. Blaauw, B., Canato, M., Agatea, L., Toniolo, L., Mammucari, C., Masiero, E., Abraham, R., Sandri, M., Schiaffino, S., and Reggiani, C. (2009). Inducible activation of Akt increases skeletal muscle mass and force without satellite cell activation. FASEB J. *23*, 3896–3905. https://doi.org/10.1096/fj.09-131870.

82. Schindelin, J., Arganda-Carreras, I., Frise, E., Kaynig, V., Longair, M., Pietzsch, T., Preibisch, S., Rueden, C., Saalfeld, S., Schmid, B., et al.

(2012). Fiji: an open-source platform for biological-image analysis. Nat. Methods *9*, 676–682. https://doi.org/10.1038/nmeth.2019.

83. Rozen, S., and Skaletsky, H. (2000). Primer3 on the WWW for general users and for biologist programmers. Methods Mol. Biol. *132*, 365–386. https://doi.org/10.1385/1-59259-192-2:365.

84. Korb, O., Stützle, T., and Exner, T.E. (2009). Empirical scoring functions for advanced protein-ligand docking with PLANTS. J. Chem. Inf. Model. *49*, 84–96. https://doi.org/10.1021/ci800298z.

85. Maier, J.A., Martinez, C., Kasavajhala, K., Wickstrom, L., Hauser, K.E., and Simmerling, C. (2015). ff14SB: Improving the Accuracy of Protein Side Chain and Backbone Parameters from ff99SB. J. Chem. Theory Comput. *11*, 3696–3713. https://doi.org/10.1021/acs.jctc.5b00255.

86. Harvey, M.J., Giupponi, G., and Fabritiis, G.D. (2009). ACEMD: Accelerating Biomolecular Dynamics in the Microsecond Time Scale. J. Chem. Theory Comput. *5*, 1632–1639. https://doi.org/10.1021/ct9000685.

87. Bonora, M., Giorgi, C., Bononi, A., Marchi, S., Patergnani, S., Rimessi, A., Rizzuto, R., and Pinton, P. (2013). Subcellular calcium measurements in mammalian cells using jellyfish photoprotein aequorin-based probes. Nat. Protoc. *8*, 2105–2118. https://doi.org/10.1038/nprot.2013.127.

Please cite this article in press as: Gherardi et al., Mitochondrial calcium uptake declines during aging and is directly activated by oleuropein to boost energy metabolism and skeletal muscle performance, Cell Metabolism (2024), https://doi.org/10.1016/j.cmet.2024.10.021



## STAR★METHODS

### KEY RESOURCES TABLE

| REAGENT or RESOURCE | SOURCE | IDENTIFIER |
|---|---|---|
| Antibodies | | |
| Rabbit monoclonal anti-MCU | Cell Signaling Technology | Cat#14997; RRID:AB_2721812 |
| Rabbit polyclonal anti-MCUR | Booster | Cat#A08547-1 |
| Mousse monoclonal anti-TOM20 (F-10) | Santa Cruz | Cat#sc-17764; RRID:AB_628381 |
| Rabbit polyclonal anti-MICU1 | Sigma Aldrich | Cat#HPA037479; RRID:AB_2675495 |
| Rabbit polyclonal anti-PDH | Cell Signaling Technology | Cat#2784; RRID:AB_2162928 |
| Rabbit polyclonal anti-PDH (phospho S293) | Abcam | Cat#ab92696, RRID:AB_10711672 |
| Rabbit monoclonal anti-TOM20 (D8T4N) | Cell Signaling Technology | Cat#42406, RRID:AB_2687663 |
| Mouse monoclonal anti-GRP 75 (D-9) | Santa Cruz Biotechnology | Cat#sc-133137, RRID:AB_2120468 |
| Anti-Rabbit Detection Module | ProteinSimple | Cat#DM-001 |
| Rabbit polyclonal anti_MCUR1 | Cell Signaling Technology | Cat#13706S; RRID:AB_2749813 |
| Chemicals, peptides, and recombinant proteins | | |
| ATP | Sigma Aldrich | Cat#A9187; CAS #: 74804-12-9 |
| Histamine | Sigma Aldrich | Cat#H7125; CAS #: 51-45-6 |
| Caffeine | Sigma Aldrich | Cat#C0750; CAS #: 58-08-2 |
| Epibatidine | Sigma Aldrich | Cat#E1145;CAS #: 16637-43-2 |
| Oleuropein | Extrasynthese | Cat#0228S; CAS #:32619-42-4 |
| Oleuropein Aglycone | Toronto Research Chemicals | Cat#O532945; CAS #:31773-95-2 |
| Hydroxytyrosol | Extrasynthese | Cat#4999S; CAS #: 10597-60-1 |
| Oligomycin | Sigma Aldrich | Cat#75351 |
| FCCP | Sigma Aldrich | Cat#C2920 |
| Rotenone | Sigma Aldrich | Cat#45656 |
| AntimycinA | Sigma Aldrich | Cat#A8674 |
| Calcein AM | Sigma Aldrich | Cat#C0875; CAS#: 154071-48-4 |
| Human Fibronectin | Corning | Cat#356008 |
| PhosSTOP | Merck | Cat#4906845001 |
| Fura-2, AM, cell permeant | Thermo Fisher | Cat#F1221 |
| Gibco™ MEM, GlutaMAX™ Supplement | Thermo Fisher | Cat#41090 |
| GOOD fetal bovine serum - 500 ml | PanBiotech | Cat#P40-37500 |
| Penicillin-Streptomycin (5,000 U/mL) | Thermo Fisher | Cat#15070063 |
| Gibco™ DMEM, high glucose, GlutaMAX™ Supplement, pyruvate | Thermo Fisher | Cat#31966 |
| Gibco™ DMEM, high glucose, HEPES | Thermo Fisher | Cat#42430 |
| Complete, Mini EDTA-free Protease Inhibitor Cocktail | Merck | Cat#11836170001 |
| RIPA lysis and extraction buffer | Thermo Fisher | Cat#89901 |
| Non-Fat Dry Milk | BioRad | Cat#100-04504 |
| PBS 1X PH 7.4 | Thermo Fisher | Cat# 10010023 |
| Skeletal Muscle Cell Growth Medium | Zen-Bio | Cat#SKM-M medium |
| Dulbecco's Modified Eagle Medium F-12 Nutrient Mixture (DMEM/F-12 (1:1) (1x) +GlutaMAX) | Thermo Fisher | Cat#31331028 |
| FBS | Thermo Fisher | Cat#10270106 |
| Heat-inactivated Horse Serum | Thermo Fisher | Cat#26050088 |
| PBS | Thermo Fisher | Cat#10010023 |
| Tyrode's salts | Sigma Aldrich | Cat#T2145 |
| Dulbecco′s Modified Eagle′s Medium | Sigma Aldrich | Cat#D5030 |

(*Continued on next page*)

Please cite this article in press as: Gherardi et al., Mitochondrial calcium uptake declines during aging and is directly activated by oleuropein to boost energy metabolism and skeletal muscle performance, Cell Metabolism (2024), https://doi.org/10.1016/j.cmet.2024.10.021





*Continued*

| REAGENT or RESOURCE | SOURCE | IDENTIFIER |
|---|---|---|
| TRIzol™Reagent | Invitrogen, Thermo Fischer | Cat#15596026 |
| SuperScript™ III CellsDirect™ cDNA Synthesis Kit | Invitrogen, Thermo Fisher | Cat# 18080300 |
| Master Mix PowerTrack™ SYBR Green | Thermo Fisher | Cat# A46109 |
| Coelenterazine n | Biotium | 10110 CAS #: 55779-48-1 |
| Digitonin | Sigma Aldrich | D5628; CAS#: 11024-24-1 |
| N-Benzyl-p-toluenesulfonaMide | Sigma Aldrich | BL3H160B8B26; CAS#: 1576-37-0 |
| Sodium Chloride | Sigma Aldrich | CAS#: 7647-14-5 |
| Magnesium Chloride | Sigma Aldrich | CAS#:7791-18-6 |
| HEPES | Sigma Aldrich | CAS#: 7365-45-9 |
| Glucose | Sigma Aldrich | CAS#: 50-99-7 |
| Calcium Chloride | Sigma Aldrich | CAS#: 10043-52-4 |
| Potassium Chloride | Sigma Aldrich | CAS#: 7447-40-7 |
| Thapsigargin | Sigma Aldrich | T9033; CAS#: 67526-95-8 |
| EGTA | Sigma Aldrich | E3889; CAS#: 67-42-5 |
| Collagenase A | Roche | Cat#COLLA-RO |
| Kaempferol | Sigma Aldrich | CAS#: 5020-18-3 |
| Olive leaf extract standardized with 40% oleuropein (OLE) | Bioactor | CAS#: 8060-29-5 |
| JC-10 dye | Enzo Lifesciences | Cat#ENZ-52305 |
| Hoestch | Invitrogen | Cat#H33342 |
| Tris(2-carboxyethyl)phosphine (TCEP) | Sigma Aldrich | Cat#: C4706; CAS#: 51805-45-9 |
| **Critical commercial assays** | | |
| BCA protein assay kit | Pierce Thermo Fisher | Cat#23227 |
| 12-230kD Sally Sue Separation Module | Protein Simple | Cat#SM-S001 |
| Pyruvate dehydrogenase (PDH) Enzyme Activity Microplate Assay Kit (ab109902) | Abcam | Cat#ab109920 |
| NuPAGE™ 4 to 12%, Bis-Tris, 1.0–1.5 mm, Mini Protein Gels | Invitrogen | Cat#NP0336BOX |
| Nitrocellulose membranes | BioRad | Cat#1704158 |
| 12-230 kDa Separation Module | Protein Simple | Cat#SM-S001 |
| Incucyte® Annexin V Green Dye | Sartorius | Cat#4642 |
| **Deposited data** | | |
| RNA-sequencing data | Gene Expression Omnibus | GSE11016 |
| Source data | This paper | Data S1 Source Data |
| **Experimental models: Cell lines** | | |
| Human Skeletal Muscle Cells, Donor 7, Lot# 655307 | Lonza | Cat#LZ-CC-2580 |
| Human Skeletal Muscle Cells, Donor 29, Lot # 639629 | Lonza | Cat#LZ-CC-2580 |
| Human Skeletal Muscle Cells, Donor 215, Lot # SKM070512A | Amsbio | Cat#SKB-F |
| Human Skeletal Muscle Cells, Donor 712, Lot # SKM062712B | Amsbio | Cat#SKB-F |
| Human Skeletal Muscle Cells, Donor 211, Lot # SK120211 | Amsbio | Cat#SKB-F |
| Human Skeletal Muscle Cells, Lot# P01064-69M | Cook Myosite | Cat#SK-1111 |

(*Continued on next page*)

Please cite this article in press as: Gherardi et al., Mitochondrial calcium uptake declines during aging and is directly activated by oleuropein to boost energy metabolism and skeletal muscle performance, Cell Metabolism (2024), https://doi.org/10.1016/j.cmet.2024.10.021



*Continued*

| REAGENT or RESOURCE | SOURCE | IDENTIFIER |
|---|---|---|
| MEF cells | G. Hajnoczky (MitoCare Center, Dpt. of Pathology, Anatomy and Cell Biology, Thomas Jefferson University, Philadelphia, Pennsylvania 19107, USA) | PMID: 26956930 |
| MEF MICU1-KO cells | G. Hajnoczky (MitoCare Center, Dpt. of Pathology, Anatomy and Cell Biology, Thomas Jefferson University, Philadelphia, Pennsylvania 19107, USA) | PMID: 26956930 |
| C2C12, Muscle Mouse Myoblast | ATCC | Cat# CRL1772 Lot# 509793 |
| HeLa | ATCC | Cat# ATCC-CCL-2 |
| Recombinant DNA | | |
| Ad5-U6-shMCUR1 | Sirion Biotech | N/A |
| Ad5-CMV-Mito-Aequorin-Mutant(D119A)-polyA-SV40-Neo | Sirion Biotech | N/A |
| Ad5-U6-shRNAscramble | Sirion, Biotech | N/A |
| Ad5-U6-shMCU#1-U6-shMCU#2 | Sirion Biotech | N/A |
| Ad CMV 4mtD3cpv SV40pA | Sirion Biotech | N/A |
| pcDNA3.1-mtGCaMP6f | available upon request | https://doi.org/10.1016/j.celrep.2015.01.056 |
| pETite-6His-MICU1 | available upon request | https://doi.org/10.1016/j.celrep.2020.01.081 |
| Software and algorithms | | |
| GraphPad Prism Software 7.02 | GraphPad | N/A |
| Fiji | ImageJ | https://doi.org/10.1038/nmeth.2019 |
| Gen5 Microplate Reader and imager software | Biotek | N/A |
| XF96 instrument | Seahorse Biosciences | N/A |
| MetaXpress High-Content Image Acquisition and Analysis Software | Molecular Devices | N/A |
| FLIPR Penta High-Throughput Cellular Screening System | Molecular Devices | N/A |
| KNIME Analytics Platform | KNIME AG | N/A |
| IncuCyte® Basic Analysis software | Sartorius | N/A |
| BiacoreTM Insight Evaluation Software, | Cytiva Life Sciences | N/A |
| Other | | |
| 35 mm Dish, No 1.5 Coverslip | MatTek | Cat#P35G-1.5-20-C |
| 96 Well White Polystyrene Microplate | Corning | Cat#3903 |
| MicroWell™ 384 well optical bottom plates | Nunc | Cat#64810 |
| 96-well black plate μClear | Greiner Bio-one | Cat#655090 |
| 1 mL HisTrap Excel column | Cytiva | Cat#29048586 |
| HiLoad 26/600 Superdex 200 pg | Cytiva | Cat#28989336 |
| Vivaspin® Turbo 4 Centrifugal Concentrator (MWCO 10 kDa) | Sartorius | Cat#VS04T02 |
| Biacore™ 8K | Cytiva | Cat#29722782 |

## EXPERIMENTAL MODEL AND STUDY PARTICIPANT DETAILS

### Cell lines and primary human myotubes

HeLa cells (ATCC, #CCL-2™) were maintained in growth medium consisting of DMEM, GlutaMAX supplement Medium (MEM) (Gibco, Thermo Fisher) containing 10 % heat-inactivated FBS, 100 U/mL penicillin and 100 mg/mL streptomycin (Gibco, Thermo Fisher).

Mouse Embryonic Fibroblasts (MEF) (MitoCare Center, department of pathology, USA) and C2C12 cells (ATCC, #CRL-1772) were cultured in growth medium comprising DMEM, high glucose, GlutaMAX™ Supplement, pyruvate (Gibco, Thermo Fisher, #31966) containing 10 % heat-inactivated FBS (Gibco, Thermo Fischer, #26050088), 100 U/ml penicillin and 100 mg/ml streptomycin (Thermo

Fisher, #15070063). C2C12 cells were differentiated into myotubes using DMEM, high glucose, GlutaMAX™ supplement, pyruvate (1 mM) (Gibco, Thermo Fisher, #31966) supplemented with 2 % heat-inactivated horse serum (Gibco, Thermo Fischer, #26050088), 100 U/ml penicillin and 100 mg/ml streptomycin (Thermo Fisher, #15070063).

Primary human Skeletal Muscle cells were purchased from Lonza (#CC-2580: 655307, 639629), Amsbio (#SKB-F: SKM070512A; SK120211; SKM062712B), and Cook (#SK1111: P01477, P01064, P01590) and kept in Skeletal Muscle Cell Growth Medium (Zen-Bio, SKM-M medium). Differentiation of human myoblasts was initiated by adding DMEM/F-12 (1:1) (1x) + GlutaMAX (Gibco, Thermo Fisher, #31331028) containing 2 % heat-inactivated horse serum (Gibco, Thermo Fischer, #26050088), 100 U/ml penicillin and 100 mg/ml streptomycin (Thermo Fisher, #15070063). All cell lines were maintained at 37 °C and 5 % $CO_2$. Changes of incubation conditions are indicated in the respective methods. All primary human myoblasts were from vastus lateralis muscle of adult donors, and quality controlled for myogenic purity and ability to differentiate. The supplier received informed consent from the donors and the ethical approval for the use of the cells for this study was obtained from the Vaud ethics commission for human research (CER–VD) under protocol 281/14.

### Animals

Young (3-4 months) and aged (24 months) male C57Bl6J wildtype mice were purchased from Charles River or Janvier Labs. Aged Wistar rats aged 19 months were purchased from Janvier labs. Skeletal muscle specific MCU knockout mice (skMCU$^{-/-}$) were previously generated in the lab of Profs. Mammucari and Rizzuto as described in Gherardi et al.,[31] by crossing homozygous MCU$^{fl/fl}$ mice with transgenic mice expressing the Cre recombinase under the control of the Mlc1f promoter. All animal experiments were approved by the internal ethics committee of Nestlé. All rat studies were approved by the Office Vétérinaire. Cantonal du Canton de Vaud, Switzerland and all mouse studies were approved and performed in accordance with the Italian law D. L.vo n_26/2014. All experiments were carried out in accordance with the European Guidelines for the Care and Use of Laboratory Animals and approved. Animals were raised or acclimatized to the conditions of the animal facility, and housed in a ventilated room under a controlled temperature (21 ± 2°C), with a 12:12h light:dark cycle and free access to chow rodent diet and water ad libitum. Mouse flexor digitorum brevis (FDB) myofibers were isolated for ex vivo $Ca^{2+}$ and OCR measurements. Mouse Tibialis anterior muscles were used for RT-PCR, PDH activity assays, and western blotting.

## METHOD DETAILS

### Human skeletal muscle transcriptomics

RNA sequencing data from Singapore sarcopenia study were extensively described in Migliavacca et al.[15] and are available at the Gene Expression Omnibus (https://www.ncbi.nlm.nih.gov/geo/) under accession numbers GSE111016. Here we analyzed the expression of genes controlling mt$Ca^{2+}$ uptake and extrusion in human muscle biopsies of the vastus lateralis from older people with and without sarcopenia. Briefly, after removing genes with a mean expression lower than 20 reads, data were normalized by the trimmed mean of M-values method as implemented in the edgeR function calcNormFactors[72] and the voomWithQualityWeights function was applied to model the mean-variance relationship and estimate the sample-specific quality weights.[73] p Values were corrected for multiple testing using the Benjamini–Hochberg method. Protein interaction network was generated with the MCUR1 protein coding gene using STRING version 11.5 (http://string-db.org/), all data sources, a high confidence score of 0.7 and the maximum number of interactors shown in the first shell set to 50. The interaction network was used as input for functional enrichment analysis using Cytoscape (version 3.9.1) to decipher functionally grouped gene ontology using ClueGO.

### Mitochondrial $Ca^{2+}$ uptake in primary human skeletal muscle myotubes

Human Skeletal Muscle cells (Lonza, #CC2580) isolated from quadriceps were seeded in a previously prepared 96-well plate, coated with human fibronectin (Corning, #356008) at 20 μg/ml for 1 h at RT and washed twice with PBS 1 X (Thermo Fisher, #10010023) before Skeletal Muscle Cell Growth Medium was added together with 12 000 cells/well. After 24 h, knockdown of MCU or MCUR1 was induced by adenoviral infection with MCU shRNA or MCUR1 shRNA (Sirion Biotech, Germany) at MOI 100. Control cells were subjected to adenoviral infection with scrambled shRNA (Sirion Biotech, Germany) at MOI 100 and all are incubated for 48 h. Cells were then differentiated into myotubes by replacing the medium with Dulbecco's Modified Eagle Medium F-12 Nutrient Mixture (DMEM/F-12 (1:1) (1x) + GlutaMAX) (Thermo Fisher, #31331028) containing 2 % horse serum (Thermo Fischer, #26050088), 100 U/ml penicillin and 100 mg/ml streptomycin (Thermo Fisher, #15070063). After 3 days, cells were subjected to adenoviral infection with mitochondria-targeted aequorin (Sirion Biotech, Germany) at MOI 200 and incubated for 24 h. For experiments with oleuropein-a, myotubes were washed with aequorin buffer and incubated with native coelenterazine at 5 μM for 2 h at RT in the dark before removing coelenterazine and adding a final concentration of 10 μM Oleuropein-a in 1 % DMSO with aequorin buffer and incubating the cells for 20 min at RT in the dark. Control myotubes were treated with DMSO 1% in aequorin buffer. Myotubes were stimulated with 5 mM caffeine.

### Mitochondrial $Ca^{2+}$ uptake in human skeletal muscle myotubes from healthy and sarcopenic donors

#### *Study Design*

Participants were recruited from the UK Hertfordshire Sarcopenia Study (HSS), a sub-study of the Hertfordshire Cohort Study (HCS). The HSS is a UK birth cohort designed to investigate lifecourse influences on later life health. From 2012-2015, 168

community-dwelling men and women aged around 78 years were recruited to study muscle function, herein termed the Hertfordshire Sarcopenia Study extension (HSSe)[74]; 142 participants had quadriceps biopsy muscle tissue from which satellite cells were isolated. Participants gave written informed consent, and the study was approved by the Hertfordshire Research Ethics Committee (07/Q0204/68). Skeletal Muscle Stem Cell Isolation and Myoblast Culture. All samples were processed within 1 hour of muscle biopsy. Biopsies were minced, then digested in 0.5 mg/ml collagenase (Sigma) in serum free DMEM (Gibco) at 37°C for 20 min with agitation. Samples were then centrifuged and resuspended in PBS and subsequently filtered through a 100μM cell strainer (BD Falcon). Cells were centrifuged again and resuspended in proliferation medium. Next, the cells were pre-plated onto 10 cm dishes and incubated at 37°C for 3 hours to permit any fibroblasts to attach. Cells and media were then transferred to 10 cm matrigel coated dishes (Corning) and incubated for 48 hours. To enrich the myogenic population, cells were sorted using CD56 MicroBeads (Miltenyi Biotech) according to the manufacturer's instructions. Cells at passage 4 were differentiated for Mitochondrial $Ca^{2+}$ analysis. Mitochondria $Ca^{2+}$ uptake was measured as described in the previous section. Luminescence was quantified at a plate reader Flexstation 3, Molecular Devices.

### High throughput screening of mitochondrial $Ca^{2+}$

The high throughput screening includes a primary and an orthogonal screen of $mtCa^{2+}$ and a secondary screen of cytosolic $Ca^{2+}$. Mitochondrial and cytosolic $Ca^{2+}$ concentrations were measured in intact HeLa cells by using the luminescent signal of the mitochondrial- and cytosolic-targeted $Ca^{2+}$ sensors aequorin.[75] 9 000 cells/well were seeded in 384-well plates (Corning, #3903) and 15 000 cells/well were seeded in 96 well plates (Corning, #64810), in standard growth medium. After 24 h, HeLa cells were infected with 200 MOI (multiplicity of infection) of the adenoviral vector (Sirion Biotech, Germany) carrying either mitochondria-targeted aequorin[76] for primary and orthogonal screening or the cytosolic-targeted aequorin[77] for counter screening. After 48 h, the medium was removed and the cells were incubated with 5 μM native coelenterazine (Biotium, #10110-1) diluted in aequorin buffer (145 mM NaCl, 1 mM $MgCl_2$, 5 mM KCl, 10 mM HEPES, 10 mM glucose, 1 mM $CaCl_2$, pH 7.4) for 2 h at RT in the dark. Then, coelenterazine was aspired and pure compounds were added at 10 μM final concentration in DMSO 1 % for 2 h at RT in the dark. Luminescent signal was measured, in basal condition and after stimulation with 100 μM Histamine (Merck, #7125), diluted in aequorin buffer. To calibrate the $Ca^{2+}$ bioluminescence, HeLa cells were semi-permeabilized with 25 μM digitonin (Merck, #11024-24-1) and 10 mM $CaCl_2$ (Merck, #21115) in aequorin buffer. Biolumiscence was detected at the plate readers FLIPR TETRAmax (Molecular Device, USA) and Cytation 3 (Biotek, USA) for 384 well format and 96 well plates format, respectively. The screening library was assembled internally from commercially available natural products that have been reported in food in the Dictionary of Food Compounds.[78] This dictionary contains entries describing natural components of food raw materials and food products and is available at https://dfc.chemnetbase.com/faces/chemical/ChemicalSearch.xhtml.

### Mitochondrial $Ca^{2+}$ uptake in C2C12 cells and Mouse Embryonic Fibroblasts (MEFs)

C2C12 cells (ATCC, #CRL-1772) were seeded in a 384-well plate with 4500 cells/well, in respective growth medium. After 24 h, cells were differentiated into myotubes by replacing the medium with Dulbecco's Modified Eagle Medium GlutaMAX Supplement High Glucose + Pyruvate (Thermo Fisher, #31966) containing 2 % heat-inactivated horse serum (Thermo Fischer, #26050088), 100 U/ml penicillin and 100 mg/ml streptomycin (Thermo Fisher, #15070063). After 3 days of incubation, cells were subjected to adenoviral infection with mitochondria-targeted aequorin (Sirion Biotech, Germany) at MOI 100 and incubated for 48 h. $mtCa^{2+}$ uptake was determined according to the general protocol using 5 mM caffeine (Sigma Aldrich, #C0750) as stimulant to trigger $Ca^{2+}$ release from the sarcoplasmic reticulum.

For measurements of mitochondrial $Ca^{2+}$ uptake in $MICU1^{-/-}$ MEFs 250 000 cells /well were seeded in a 6-well plate. After 24h, cells were transfected with mitochondria-targeted aequorin plasmids using Lipofectamine 3000 (Thermo Fisher), according to the manufacturer's instruction. The cells were replated into 96-well plates (1:6 dilution) the day before the experiment. After reconstitution with 5 μM coelenterazine, cells were placed in 70 μl of Krebs-Ringer modified buffer (KRB) (125 mM NaCl, 5 mM KCl, 1 mM $MgCl_2$, 20 mM HEPES, 1 mM $MgSO_4$, 0.4 mM $KH_2PO_4$, 1 mM $CaCl_2$, 5.5 mM glucose, pH 7.4) supplemented with 1 mM $CaCl_2$ at 37°C, containing 10 μM compounds or 0.1% DMSO and luminescence from each well was measured for 1 min. During the experiment, 500 μM ATP was first injected to activate calcium transients, then a hypotonic, $Ca^{2+}$-rich, digitonin-containing solution (10 mM $CaCl_2$ in $H_2O$) was added to discharge the remaining aequorin pool. The light signal was collected and calibrated into $[Ca^{2+}]$ values by an algorithm based on the $Ca^{2+}$ response curve of aequorin at physiological conditions of pH, $[Mg^{2+}]$ and ionic strength, as described in the section "data analysis"[79].

### Mitochondrial $Ca^{2+}$ uptake in semi-permeabilized HeLa cells

To measure $mtCa^{2+}$ uptake in semi-permeabilized HeLa (ATCC, #CCL-2™) and MEF cells[53] 35 000 cells/well and 15 000 cells/well respectively were seeded in 96 well plates. After 24 h, cells were infected with the mitochondria-targeted aequorin probe as described in the previous section. After 2 h of incubation with native coelenterazine (Biotium, USA, #10110-1) at 5 μM, cells were washed and first treated with a thapsigargin (Sigma Aldrich, #T9033) solution (0.2 μM) containing intracellular medium (IM: 140 mM KCl, 1 mM $KH_2PO_4$, 1 mM $MgCl_2$ and 20 mM Na-HEPES) supplemented with 10 mM Glucose and 0.1 mM EGTA (Sigma Aldrich, #E3889) at pH 7.2 for 15 min. 5 min before starting the measurement, a 60 μM digitonin (Sigma Aldrich, #D5628) solution containing DMSO 1 % for control or 10 μM of the selected compound (in 1 % DMSO) for the treated samples, was added. Basal luminescence was measured before stimulating the cells with intracellular medium supplemented with 8 mM Na-Succinate, 4 mM

Na-Pyruvate, 4 mM Mg-ATP, 5 mM Mg-EDTA, and 4μM free $Ca^{2+}$. Free [$Ca^{2+}$] was calculated with the Maxchelator program. Finally, a calibration solution containing 140 mM KCl and 10 mM $CaCl_2$ was used to calibrate the signal[48]. Slope values of $mtCa^{2+}$ were analyzed during the linear phase of the uptake.

### MICU1 protein expression and purification, and determination of Oleuropein binding by Surface Plasmon Resonance (SPR)

6xHis-tagged MICU1 was recombinantly expressed in *Escherichia coli* ShuffleT7 cells, transformed with the pETite-6His-MICU1 plasmid. An overnight pre-inoculum of transformed cells in LB medium supplemented with 30 μg/mL kanamycin and 30 μg/mL spectinomycin was used to inoculate fresh LB medium supplemented with 50 μg/mL kanamycin. Cells were grown at 37 °C and protein overexpression was induced adding 1mM IPTG to cultures in the late-exponential growth phase ($OD_{600nm}$ > 1.2). Protein expression was carried out for 3h at 37 °C. Bacterial cell pellet was resuspended in Buffer A (20 mM HEPES, 500 mM NaCl, 1 mM $CaCl_2$, 0.1mM TCEP, 10% v/v glycerol, pH 7.5) supplemented with 0.05% v/v Triton-X100, 1X Protease Inhibitor Cocktail (Serva), 10U of DNAse I and Lysozyme and lysed by a One Shot Cell Disruptor (Constant Systems, Ltd.) operated at 1.35 kBar. Cell debris were removed by centrifugation and the lysate soluble fraction was loaded on a 1 mL HisTrap Excel column (Cytiva). After extensive washing of the resin by buffer A, 6xHis-tagged MICU1 was eluted by a linear gradient of Buffer B (20 mM HEPES, 250 mM NaCl, 1 mM $CaCl_2$, 0.1mM TCEP, 10% v/v glycerol, 500 mM Imidazole, pH 7.5; 0-100% in 15 column volumes). The fractions of interest were further purified via size-exclusion chromatography by a HiLoad Superdex200 26/600 preparation grade column (Cytiva) equilibrated in 20 mM HEPES, 250 mM NaCl, 1 mM $CaCl_2$, 0.1 mM TCEP, 10% v/v glycerol, pH 7.0. Mostly pure fractions (as revealed by SDS-PAGE) were pooled together and concentrated to 0.2-0.5 mg/mL by a Vivaspin Turbo 4 ultrafiltration device (MWCO 10 kDa; Sartorius). Recombinant 6xHis-tagged MICU1 was obtained at a high level of purity (>90 %) and at a sufficient yield for SPR experiments. As evidenced by the retention volumes in size exclusion chromatography, MICU1 exists in solution mostly as a dimer. Since the presence of $Ca^{2+}$ cations is known to favor MICU1 dimeric form and to destabilize higher order aggregates (i.e. hexamers, [80]), it has been kept in the storage buffer and in the SPR running buffer.

The binding of oleuropein to MICU1 was measured via surface plasmon resonance, by a Biacore 8k (Cytiva) operated with a running buffer including 20 mM HEPES, 250 mM NaCl, 0.2 mM $CaCl_2$, 0.005% v/v Tween-20, 1% v/v DMSO, pH 7.0. Purified MICU1 was diluted to 30 μg/mL in 10 mM sodium acetate, pH 4.2 and immobilized on a Series S CM5 sensor chip (Cytiva) via amine coupling, reaching between 8000 and 12000 RUs. A flow cell with no immobilized protein was used as reference.

Serial dilutions of Oleuropein in running buffer were injected over the active and reference flow cells in single-cycle kinetic experiments (30 μL/min flowrate, 120 s of contact time and 600 s of dissociation). Blank runs were performed by injecting only running buffer. A 4-point solvent correction was performed to screen for possible interference by DMSO. The experiment was conducted in duplicate on newly immobilized MICU1. Double referenced and solvent-corrected sensorgrams were analyzed by the Biacore Insight Evaluation Software, fitting experimental data to a 1:1 binding model and obtaining the steady-state *kd*. Further data processing was performed by GraphPad Prism 8. The experimental conditions have been validated by measuring the affinity of a known binder of MICU1 (MCU-i11; measured *kd* = 3.7 ± 0.8 μM), obtaining a value compatible with previously measured results.[50]

### Mitochondrial respiration in primary human myotubes

To measure the effect of oleuropein aglycone on oxygen consumption rate (OCR) in control and MCU-knockdown human myotubes, 8 000 cells/well were seeded in a respective Seahorse XF96 Cell Culture Microplate (Agilent, #101085-004) previously coated with fibronectin (Corning, #356008) at 20 μg/ml for 1 h at RT and washed twice with PBS 1X (Thermo Fisher, # 10010023) before adding the cells and incubating them overnight. The next day, cells were infected with 100 MOI of adenoviral MCU shRNA (Sirion Biotech, Germany) to induce knockdown of MCU. Control cells were infected with 100 MOI of scrambled shRNA (Sirion Biotech, Germany). After 48 h, cells were differentiated into myotubes by exchanging the medium with DMEM/F-12 (1:1) (1x) + GlutaMAX (Thermo Fisher, #31331028) containing 2 % horse serum (Thermo Fisher, #31331028), 100 U/ml penicillin and 100 mg/ml streptomycin (Thermo Fisher, #15070063). After 72 h, cells were washed with KRBH and incubated with 10 μM oleuropein-a (Toronto Chemicals, #O532945) in 1 % DMSO for 20 min at 37 °C without extra $CO_2$. For the acquisition, basal respiration was recorded before injecting caffeine (Sigma Aldrich, #C0750) at final concentration 5 mM to stimulate the myotubes followed by 2.5 μg/ml oligomycin (oligo, Sigma Aldrich, #75351) and 2 μM rotenone (rot, Sigma Aldrich, #45656) plus 2 μg/ml antimycin A (AntiA, Sigma Aldrich, #A8674). Basal respiration of control and MCU-kd myotubes was used for normalization and expressed in % to see the effect of oleuropein-a on OCR.

### Cell Death in primary human myotubes

To monitor apoptosis in Human Primary HSMM, 15 000 cells/well were seeded in a 96-well μClear black plate pre-coated with 20 μg/ml of fibronectin. After 24 h, cells were differentiated into myotubes by replacing the medium with DMEM/F-12 (1:1) (1x) + GlutaMAX (Thermo Fisher, #31331028) containing 2% heat-inactivated horse serum (Thermo Fischer, #26050088), 100 U/ml penicillin and 100 mg/ml streptomycin (Thermo Fisher, #15070063) and incubated for 3 days. Cells were stained with Incucyte Annexin V Green Dye (Sartorius) according to manufacturer's instructions. Then, they were treated with Oleuropein, Oleuropein aglycone at 10 μM, and Staurosporin at 100nM, and the plate was placed into the Incucyte Zoom incubator (Sartorius) to acquire green fluorescence (Ex: 490nm, Em: 515 nm) and contrast phase every 4 hours for 24h. The quantification of phase and fluorescent object in real-time were analyzed with The IncuCyte Basic Analysis software.

### Single-cell imaging of mitochondrial Ca2+ signals

Mitochondrial Ca2+ was measured with the genetically encoded cameleon sensors. 150 000 cells/dish of C2C12 cells were plated on fibronectin-treated 35-mm-diameter glass-bottom dishes (MatTek, MA). After 24 h, cells were differentiated into myotubes by replacing the medium with Dulbecco's Modified Eagle Medium GlutaMAX Supplement High Glucose + Pyruvate (Thermo Fisher, #31966) containing 2 % heat-inactivated horse serum (Thermo Fischer, #26050088), 100 U/ml penicillin and 100 mg/ml streptomycin (Thermo Fisher, #15070063). After 4 days of incubation, cells were infected with adenovirus encoding a mitochondria-cameleon sensors 4mt3CpV (Sirion Biotech, Germany) at MOI 100 and incubated for 48h. Myotubes were washed three times and experiments were performed at 37°C in KRBH buffer containing (in mM): 140 NaCl, 3.6 KCl, 0.5 NaH2PO4, 0.5 MgSO4, 1.5 CaCl2, 10 HEPES, 5 NaHCO3, 10 Glucose (pH 7.4). Glass coverslips were inserted in a thermostatic chamber (Life Imaging Services). Cells were imaged on a DMI6000 B inverted fluorescence microscope, using a HCX PL APO 40×1.30 NA oil immersion objective (Leica Microsystems) and an Evolve 512 back-illuminated CCD with 16×16 μm pixel camera (Photometrics, Tucson, Arizona). Cells were excited at 430 nm through a BP436/20 filter. The two emission images were sequentially acquired with BP480/40 and BP535/30 emission filters. Fluorescence ratios were calculated in MetaFluor 7.0 (Meta Imaging Series) and analyzed in Excel (Microsoft) and GraphPad Prism 7 (GraphPad). Images were taken every 2 s. Ratio data were normalized to a baseline setting of 1. The change in ratio (ΔR/R0) was calculated as the difference between the baseline value and the effect of the added compound after 5 min of treatment and stimulated with 5mM of caffeine.

### Mitochondrial membrane potential

Mitochondrial membrane potential (MMP) was assessed using JC-10 (Enzo Life Sciences, Farmingdale, NY, USA). C2C12 cells were seeded at 18 000 cells/well in 96-well μClear plate and myotubes were differentiated as described in the section "mitochondrial respiration in primary human myotubes". Nuclei were stained with Hoestch (Invitrogen) in culture medium and then, incubated with 3 μg/ml of JC10 in KRBH buffer for 15 min. Myotubes were treated with Oleuropein, Oleuropein aglycone and FCCP and stimulated with 5 mM Caffeine after JC-10 labeling. Live cells were directly imaged with a 10x objective using ImageXpress Confocal (Molecular Device). Two sites per well were acquired, and images were segmented to recognize the cells. The total intensity of both FITC and TRITC fluorescence were recorded for each cell and used to calculate the ratio of aggregated to monomer JC-10 (590 nm/525 nm). After segmentation, data were analyzed using KNIME software.

### Ex vivo muscle force and fatigue

EDL (Extensor digitorum longus) muscles were dissected from tendon to tendon under a stereomicroscope and mounted between a force transducer (KG Scientific Instruments, Heidelberg, Germany) in a small chamber in which oxygenated Krebs solution was continuously circulated and temperature maintained at 25°C. The stimulation conditions were optimized, and the length of the muscle was increased until force development during a 90Hz stimulation was maximal. The force-frequency relationship was recorded by performing muscle activation at increasing frequencies every 15 seconds, starting with a single pulse (twitch), to trains of stimuli at various rates producing unfused or fused tetani (20 Hz, 40Hz, 55Hz, 75Hz, 100Hz, 150Hz). Force was normalized for muscle weight. Oleuropein was added to the medium at a final concentration of 10 μM after the measurement of the first force-frequency relationship. After one hour, we performed a fatigue protocol which consisted of 5 tetanic contractions (100Hz) with a duration of 300ms repeated every second. Fatigue was determined as the force reduction relative to the initial force.

### In vivo treatments with Oleuropein

Animals were treated orally with an Oleuropein-rich olive leaf extract (OLE) standardized with 40% of Oleuropein as previously reported.[55] Acute single dose administration was performed by an oral gavage of 50mg/kg OLE dissolved in water, or vehicle, and skeletal muscle was collected after euthanasia 2 to 8h post gavage. Chronic OLE administration was performed via dietary exposure by feeding animals orally with an OLE-diet delivering an OLE intake of 50mg/kg/day in mice and 25mg/kg/day in rats, both corresponding to a human dose of 250mg/day after allometric scaling. Diets were prepared by SAFE, France using an AIN93 purified rodent chow diet supplemented with OLE at 0.44 g/kg for young mice, 0.69 g/kg for aged mice and 0.65 g/kg for aged rats to deliver the intended daily doses based on body weight and food intake of each cohort. Exercise performance on a treadmill was performed non invasively after 2 weeks and force and sample collection were performed after 4 weeks of OLE treatment. After euthanasia, skeletal muscle was quickly dissected and processed freshly or snap frozen in liquid nitrogen and stored at -80°C.

### In vivo DNA transfection of skeletal muscle

For muscle specific genetic over-expression in mice, a plasmid encoding the genetic calcium sensor targeted to mitochondria 4mtGCaMP6f $Ca^{2+}$ (for measurement of $mtCa^{2+}$ uptake) or the MCUR1 cDNA (for MCUR1 rescue experiments) was electroporated to FDB muscles. Mice were anesthetized and hyaluronidase solution (2mg/ml) (Sigma) was injected under the hindlimb footpads. After 30 min, 20 μg of plasmid DNA in 20 μl of physiological solution was injected with the same procedure of the hyaluronidase. Then, one gold-plated acupuncture needle was placed under the skin at heel, and a second one at the base of the toes, oriented parallel to each other and perpendicular to the longitudinal axis of the foot and connected to the BTX porator (Harvard apparatus). The muscles were electroporated by applying 20 pulses, 20 ms each, 1 s of interval to yield an electric field of 100 V. Single fibers cultures were carried out 7 days later.

### In vivo muscle force, fatigue and exercise performance

*In vivo* determination of force and contraction kinetics of gastrocnemius was carried out as shown previously.[81] Briefly, mice were anesthetized by a mixture of Rompum and Zoletil and a small incision was made from the knee to the hip, exposing the sciatic nerve. Before branching of the sciatic nerve, Teflon-coated 7 multistranded steel wires (AS 632; Cooner Wire Company, Chatsworth, CA, USA) were implanted with sutures on either side of the sciatic nerve. To avoid recruitment of the ankle dorsal flexors, and therefore significant reduction of torque, the common peroneal nerve was cut. Torque production of the stimulated plantar flexors was measured using a muscle lever system (Model 305C; Aurora Scientific, Aurora, ON, Canada). The force-frequency curves were determined by stepwise increasing stimulation frequency, pausing 30s between stimuli to avoid effects due to fatigue. Fatigue was determined as the force reduction relative to the initial force. The fatigue protocol consisted of six 100 Hz trains of 0.5s once every second. Force was calculated from the torque, assuming an average distance of 2.1 mm between the Achilles tendon insertion and ankle joint. Force was normalized for muscle weight.

Exercise performance was assessed by maximal treadmill running time. For acute concentric exercise studies, mice were acclimated to and trained on a 10° uphill LE8700 treadmill (Harvard apparatus) for 2 days. On day 1 mice ran for 5 min at 8 m min−1 and on day 2 mice ran for 5 min at 8 m min−1 followed by another 5 min at 10 m min−1. On day 3, mice were subjected to a single bout of running starting at the speed of 10 m min−1. 10 min later, the treadmill speed was increased at a rate of 1 m min−1 every 5 min until mice were exhausted. Exhaustion was defined as the point at which mice spent more than 5 s on the electric shocker without attempting to resume running. Total running time was recorded for each mouse.

### Real time imaging of mitochondrial and cytosolic $Ca^{2+}$ in FDB fibers

Real-time imaging. Muscles were digested in collagenase A (4 mg/ml) (Roche, #COLLA-RO) dissolved in Tyrode's salt solution (pH 7.4) (Sigma Aldrich, # T2145) containing 10 % fetal bovine serum (Pan Biotech, #P40-37500). Single fibers were isolated, plated on laminin-coated glass coverslips and cultured in DMEM with HEPES (Thermo Fisher, #42430), supplemented with 10 % fetal bovine serum (Pan Biotech, #P40-37500), containing 100 U/ml penicillin and 100 mg/ml streptomycin (Thermo Fisher, #15070063). Fibers were maintained in culture at 37 °C with 5 % $CO_2$.

mt$Ca^{2+}$ measurements. During the experiments, myofibers were maintained in Krebs-Ringer modified buffer (135 mM NaCl, 5 mM KCl, 1 mM MgCl2, 20 mM HEPES, 1 mM $MgSO_4$, 0.4 mM $KH_2PO_4$, 1 mM $CaCl_2$, 5.5 mM glucose, pH 7.4) containing 0.02 % pluronic acid for 20 min at 37°C and then washed with Krebs-Ringer modified buffer in presence of 75 μM N-benzyl-P-toluenesulfonamide (Sigma Aldrich, #BL3H160B8B26) to avoid the fiber contraction. 30 mM caffeine (Sigma Aldrich, #C0750) was added when indicated to elicit $Ca^{2+}$ release from intracellular stores. Experiments were performed on a Zeiss Axiovert 200 microscope equipped with a 40×/1.3 N.A. PlanFluor objective. Excitation was performed with a DeltaRAM V high-speed monochromator (Photon Technology International) equipped with a 75 W xenon arc lamp. Images were captured with a high-sensitivity Evolve 512 Delta EMCCD (Photometrics). The system is controlled by MetaMorph 7.5 (Molecular Devices) and was assembled by Crisel Instruments.

To measure mt$Ca^{2+}$ uptake in young and aged animals, fibers were dissected and loaded with 2 μM mt-fura-2/AM.[24] Images were collected by alternatively exciting the fluorophore at 340 and 380 nm and fluorescence emission recorded through a 515/30 nm band-pass filter (Semrock). Exposure time was set to 100 ms. Acquisition was performed at binning 1 with 200 of EM gain. Image analysis was performed with Fiji distribution of the ImageJ software.[82] Images were background subtracted. Changes in fluorescence (340/380 nm ratio) were expressed as R/R0, where R is the ratio at time t and R0 is the ratio at the beginning of the experiment.

To measure mt$Ca^{2+}$ uptake in oleuropein related experiments, FDB fibers were isolated 7 days after *in vivo* transfection with a plasmid encoding 4mtGCaMP6f.[31] Muscles were digested as described above. 4mtGCaMP6f was alternatively excited every second at 475 and 410 nm respectively and images were acquired through an emission filter (535/30 nm) (Chroma). Exposure time was set to 50 ms. Acquisition was performed at binning 1 with 200 of EM gain. Image analysis was performed with Fiji distribution of the ImageJ software.[82] Images were background corrected frame by frame by subtracting the mean pixel value of a cell-free region of interest. Changes in $Ca^{2+}$ levels (475/410 nm fluorescence ratio) were expressed as R/R0, where R is the ratio at time t and R0 is the ratio at the beginning of the experiment. mt$Ca^{2+}$ peak was expressed as (R-R0)/R0 and normalized for the control value.

For cytosolic $Ca^{2+}$ measurements, fibers were dissected and loaded with 2 μM fura-2/AM (Thermo Fisher, #F1221) diluted in Krebs-Ringer modified buffer (described above) containing 0.02 % pluronic acid for 20 min at 37 °C and then washed with Krebs-Ringer modified buffer in presence of 75 μM N-benzyl-P-toluenesulfonamide (Sigma Aldrich, #BL3H160B8B26) to avoid the fiber contraction. 30 mM caffeine (Sigma Aldrich, #C0750) was added when indicated to elicit $Ca^{2+}$ release from intracellular stores. Experiments were performed on a Zeiss Axiovert 200 microscope equipped with a 40×/1.3 N.A. PlanFluor objective. Excitation was performed with a DeltaRAM V high-speed monochromator (Photon Technology International) equipped with a 75 W xenon arc lamp. Images were captured with a high-sensitivity Evolve 512 Delta EMCCD (Photometrics). The system is controlled by MetaMorph 7.5 (Molecular Devices) and was assembled by Crisel Instruments. Images were collected by alternatively exciting the fluorophore at 340 and 380 nm and fluorescence emission recorded through a 515/30 nm band-pass filter (Semrock). Exposure time was set to 100 ms. Acquisition was performed at binning 1 with 200 of EM gain. Image analysis was performed with Fiji distribution of the ImageJ software.[82] Images were background subtracted. Changes in fluorescence (340/380 nm ratio) was expressed as R/R0, where R is the ratio at time t and R0 is the ratio at the beginning of the experiment.

### Mitochondrial respiration in mouse FDB fibers

For measurements of oxygen consumption rate (OCR) from *in vivo* studies, FDB fibers were mechanically isolatedin collagenase A-containing (4 mg/ml) (Roche, #COLLA-RO) Tyrode's salt solution (pH 7.4) (Sigma Aldrich, #T2145) containing 10 % fetal bovine serum (Pan Biotech, # P40-37500). Single fibers were isolated, plated on laminin-coated XF24 microplate wells and cultured in DMEM (Sigma Aldrich, # D5030), supplemented with 1 mM NaPyr, 5 mM glucose, 33 mM NaCl, 15 mg phenol red, 25 mM HEPES, 1 mM of L-Glutamine. Fibers were maintained for 2h in culture at 37 °C in 5 % $CO_2$.

To measure exogenous FA utilization, the fibers were cultured in DMEM (Sigma Aldrich, #D5030), supplemented with 0.1 mM NaPyr, 5 mM glucose, 33 mM NaCl, 15 mg phenol red, 25 mM HEPES, 1 mM of L-Glutamine, 0.5 mM carnitine and 100 μM palmitate:BSA. Fibers were maintained for 2 h in culture at 37 °C in 5 % $CO_2$.

The rate of oxygen consumption was assessed in real-time with the XFe24 Extracellular Flux Analyzer (Agilent), which allows to measure OCR changes after up to four sequential additions of compounds. Fibers were plated as reported above. A titration with the uncoupler FCCP (Sigma Aldrich, #C2920) was performed, in order to utilize the FCCP concentration (0.6 μM) that maximally increases OCR.

The results were normalized for the fluorescence of calcein (Sigma-Aldrich, #C0875). Fibers were loaded with 2 μM calcein for 30 min. Fluorescence was measured using a Perkin Elmer EnVision plate reader in well scan mode using 480/20 nm filter for excitation and 535/20 nm filter for emission.

### Genomic DNA extraction from skeletal muscle and mtDNA quantification

20 mg of skeletal muscle were incubated with shaking at 50°C o.n. in a buffer containing 100mM NaCl, 10 mM TrisHCl pH 8, 25 mM EDTA pH 8, 0.5% SDS, 0.1 mg7mL Proteinase K and the DNA was extracted with an equal volume of phenol/chloroform/isoamyl alcohol. Samples were centrifuged 10 min at 1700 g, and 2 vol of ethanol and ½ vol of 7.5 M ammonium acetate were added to the aqueous layer resulted by the centrifugation. The DNA was pelleted by centrifugation at 1700 g for 2 min. Finally, the pellet was rinsed with 70% ethanol, and resuspended at 1 mg/ml in TE buffer. Real-time PCR was performed using the QuantStudio5 Real-Time PCR System thermocycler and SYBR green chemistry (Thermo Fisher, #A46109). The following primers were used to amplify mtDNA and nuclear DNA, respectively:

mNd4-fw: TCGCCTACTCCTCAGTTAGCCA
MNd4-rv: GATGTGAGGCCATGTGCGATT
RnaseP-fw: GCCTACACTGGAGTCGTGCTAC
RnaseP-rv: CTGACCACACGAGCTGGTAGAA

### PDH activity

PDH activity was measured in freshly isolated TA muscles with the Pyruvate Dehydrogenase Enzyme Activity Microplate Assay Kit (Abcam, #ab109920) according to manufacturer's instructions.

### RNA extraction, reverse transcription, and qPCR

Total RNA was extracted from mouse tissues through mechanical tissue homogenization in TRIzol™ reagent (Thermo Fisher, #15596026), following manufacturer instructions. The RNA was quantified with Nanodrop (Thermo Fisher) and 1 μg of total RNA of each sample was retro-transcribed using the cDNA synthesis kit SuperScript II (Thermo Fisher, #18080300). Oligo(dT)12-18 primer (Thermo Fisher Scientific) were used as a primer for first stand cDNA synthesis with reverse transcriptase. The obtained cDNA was analyzed by Real-Time PCR using the QuantStudio5 Real-Time PCR System thermocycler and the SYBR green chemistry (Thermo Fisher, # A46109). The primers were designed and analyzed with Primer3.[83]The efficiency of all primers was between 90 % and 110 %. The housekeeping genes GAPDH was used as internal controls for cDNA normalization. For quantification, expression levels were calculated by using the $2^{-\Delta\Delta Ct}$ method.

Real-time PCR primer sequences were as follows:

MCU:
Fw 5'-AAAGGAGCCAAAAAGTCACG-3'
Rv 5'-AACGGCGTGAGTTACAAACA-3'
MCUb:
Fw 5'-GGCAGTGAAATTCCAGCTTCA-3'
Rv 5'-CGCTCTCGTCTCTTCTGGATC-3'
EMRE:
Fw 5'-GGACTCTGGGCTCTTGTCAC-3'
Rv 5'-AGAACTTCGCTGCTCTGCTT-3'
MICU1 splice variant specific (NM_144822):
Fw 5'-GCGCTTTGATGGAAAGAAAATTGC-3'
Rv 5'-TGTCTACCTCTCCGTCTCCA-3'
MICU1.1 splice variant specific (NM_001291443):
Fw 5'-CTTTGATGGAAAGGAGTTCTGGC-3'
Rv 5'-CCTCCATGTCTACCTCTCCGT-3'

MICU2:
Fw 5'-TGGAGCACGACGGAGAGTAT-3'
Rv 5'-GCCAGCTTCTTGACCAGTGT-3'
MICU3:
Fw 5'- CGACCTTCAAATCCTGCCTG-3'
Rv 5'- TCTGCGTGCTCTGACCTTAC-3'
MCUR1:
Fw 5'AGTTTTCAGCCCTCAGAGC-3'
Rv 5'-GGACTTTGGTCACTTCATCCATCA-3'
GAPDH:
Fw 5'-CACCATCTTCCAGGAGCGAG-3'
Rv 5'-CCTTCTCCATGGTGGTGAAGAC-3'

## Western blot and antibodies

To determine the expression level of MICU1 protein in control and MICU1-KO MEF cells, cells were washed twice using PBS and scraped from a 175 $cm^2$ flask to collect the lysate in 50 ml falcons on ice before centrifuging the cells at 1 500 rpm for 4 min at 4 °C. The supernatant was discarded and cells were resuspended in Mito buffer (300 mM sucrose, 10 mM Hepes, 0.5 mM EGTA, Complete EDTA-free protease inhibitor mixture (Merck, #11836170001, Germany), pH 7.4) and incubated on ice for 30 min. Cells were transferred to a 2 ml glass potter for homogenization and transferred to a 2 ml Eppendorf tube and centrifuged at 600 g for 10 min at 4 °C. Supernatant was collected in a 1.5 ml Eppendorf tube and centrifuged at 6 000 g for 10 min at 4°C to pellet the mitochondria, which were dissolved in 50 μl Mito buffer to measure protein concentration via BCA (Pierce Thermo Fisher, #23227). 20 μg of protein was separated by SDS- polyacrylamide gel electrophoresis using 4-12 % acrylamide gels (Invitrogen, #NP0336BOX) and transferred to PVDF membranes (Mini format 0.2 μm PVDF, Bio-Rad) with a semi-dry blotting protein transfer (Trans Blot Turbo, Bio-Rad). TBS-tween-washed membranes (0.5 M Tris, 1.5 M NaCl, 0.01 % Tween, pH 7.4) were blocked with 5 % BSA (Sigma Aldrich, #A2153) for 1 h at RT. The washed membranes were incubated overnight with the primary antibodies MICU1 1:400 (Sigma Life Science, #HPA037479) or TOM20 1:1000 (Cell Signaling, #42406) diluted in 1 % BSA at 4 °C. After 24 h, the washed membranes were incubated for 1 h at RT with IRDye 800 CW goat anti rabbit IgG (LI-COR Biosciences, U.S.) 1:15000 diluted in 1 % BSA. Membranes were scanned on the Odyssey scanner (LI-COR Biosciences, USA).

To determine MCU and MCUR1 protein levels in primary human myotubes, cells were lysed with RIPA buffer (ThermoFischer, #89901) supplemented with Complete EDTA-free protease inhibitor mixture (Merck, #11836170001) and phosSTOP™ (Merck, #4906845001). Protein concentrations were measured via BCA. For Western blotting detection, the Sally Sue automated capillary blotting system (ProteinSimple, San Jose, CA, USA) was applied. Samples were prepared according to the manufacturer's protocol using the Anti-Rabbit Detection Module (ProteinSimple, #DM-001) and the 12-230 kDa Sally Sue Separation Module (ProteinSimple, #SM-S001). The loading concentration was adjusted to 0.2 μg/μl using RIPA buffer. Primary antibodies used were MCU 1:30 (Cell Signaling, #14997), MCUR1 1:30 (Booster, #A08547-1) and TOM20 1:100 (Cell Signaling, #42406) diluted in the manufactorer's antibody diluent (ProteinSimple).

To monitor protein levels in mouse skeletal muscles, frozen muscles were pulverized by means of Qiagen Tissue Lyser and protein extracts were prepared in an appropriate buffer containing 50 mM Tris pH 7.5, 150 mM NaCl, 5 mM $MgCl_2$, 1 mM DTT, 10 % glycerol, 2 % SDS, 1 % Triton X-100, Complete EDTA-free protease inhibitor mixture (Roche), 1 mM PMSF, 1 mM NaVO3, 5 mM NaF and 3 mM β-glycerophosphate. 40 μg of total proteins were loaded, according to BCA quantification. Proteins were separated by SDS-PAGE electrophoresis, in commercial 4-12 % acrylamide gels (Thermo Fisher, # NP0336BOX) and transferred onto nitrocellulose membranes (Thermo Fisher, #1704158) by semi-dry electrophoretic transfer. Blots were blocked 1 h at RT with 5 % non-fat dry milk (Bio-Rad, #100-04504) in TBS-tween (0.5M Tris, 1.5M NaCl, 0.01 % Tween) solution and incubated at 4 °C with primary antibodies. Secondary antibodies were incubated 1 hr at RT. The following primary antibodies were used: MCU 1:1000 (Merck), phosphoPDH Ser293 1:5000 (Abcam, #ab92696), PDH 1:1000 (Cell Signaling, #2784), GRP75 1:1000 (Santa Cruz, #sc-133137), TOM20 1:1000 (Santa Cruz, #sc-17764). Full scans of uncropped representative blots are available in Data S1. Data S1 show unprocessed source data underlying all blots and graphs, related to Figures 1, 2, 3, 4, 5, 6, and S1–S9.

## Modeling

A 3D-model of human MICU1 (UNIPROT entry: Q9BPX6) was obtained from the experimentally solved structure of $Ca^{2+}$-free MICU1 in its hexameric form (PDB ID: 4NSC).[80] The strategy adopted to prepare the protein model and the identification of the binding site was previously reported.[50] The ligands were obtained from Pubchem (PubChem CID: 56842347; 5281544) and their partial charge calculated after semi-empirical (PM6) energy minimization using MOE 2018 (Stewart, J.J.P., 2012, MOPAC2012, version 202; http://OpenMOPAC2012.net, Stewart Computational Chemistry). Molecular docking studies were performed with plants1.2 coupled to chemPLP scoring function[84] defining as binding site a sphere placed on the model center of the mass and using a radius of 14 Å. For each run 20 output conformations were generated and analyzed by visual inspection.

Please cite this article in press as: Gherardi et al., Mitochondrial calcium uptake declines during aging and is directly activated by oleuropein to boost energy metabolism and skeletal muscle performance, Cell Metabolism (2024), https://doi.org/10.1016/j.cmet.2024.10.021



The ligand-protein complexes were prepared for MD simulations with AmberTools14,[85] assigning Gasteiger charges and General Amber Force Field (GAFF) parameters to the ligands and Amber14 partial charges and parameters to the proteins. Each system was solvated with explicit waters (TIP3P model) resulting in a tetragonal box with boundaries at least 11 Å far from any atom of the complex.

Each system was neutralized adding $Na^+/Cl^-$ ions to a final concentration of 0.1 M. Each system was subjected to 300 steps of conjugate-gradient minimization followed by 100 ps NVE and 500 ps NPT equilibration applying harmonic positional constraints (1 kcal $mol^{-1}$ $Å^{-2}$) on protein and ligands atoms. The pressure was maintained to 1 atm by Berendsen barostat and the temperature to 310 K by a Langevin thermostat. Subsequently, three replicas of 10 ns classical MD simulations in the NVT ensemble were conducted to compute MMGBSA energy and assess RMSD along the trajectory.

All MD simulations were carried out with the ACEMD engine,[86] with a time-step of 2fs, by handling the nonbonded long-range Coulomb interactions with the particle mesh Ewald summation method (PME) with a cutoff distance of 9 Å and a switching distance of 7.5 Å.

For the analysis of the docking, Chemplp Score/Norm column indicates the value obtained from a scoring function normalized on the number of heavy atoms, measuring the strength of the interaction. Our protocol was extended by using Molecular Dynamics to monitor the stability of the conformation obtained by the docking protocol (RMSD) and the quality of the interaction (MMGBSA score).

## QUANTIFICATION AND STATISTICAL ANALYSIS

### Data analysis

Data analysis and statistical tests were performed using GraphPad Prism 7.02. All data were expressed as the mean ± SEM.Individual number of replicates (n) and all original data can be found in the figure legends and source Data S1 file. Samples were statistically analyzed using parametric Student's *t*-test for two groups and ANOVA for multiple groups. Results were considered significant with alpha p-values lower than 0.05; $*p < 0.05$.

For the analysis of aequorin-based $Ca^{2+}$ data, the raw data from the Cytation3 Imaging Reader (BioTek, Switzerland) and FLIPR tetraMAX (Molecular Devices, USA) were calibrated using the following equation.[87]

$$Ca^{2+}(M) = \frac{\left(\frac{L}{L_{max}} * \lambda\right)^{\frac{1}{n}} + \left(\left(\frac{L}{L_{max}} * \lambda\right)^{\frac{1}{n}} * K_{TR}\right) - 1}{K_R - \left(\left(\frac{L}{L_{max}} * \lambda\right)^{\frac{1}{n}} * K_R\right)}$$

$L$ = light intensity at sampling time
$L_{max}$ = total light emitted at sampling time
$K_R$ = constant for calcium-bound state
$K_{TR}$ = constant for calcium-unbound state
$\lambda$ = rate constant for aequorin consumption at saturation [$Ca^{2+}$]
$n$ = number of $Ca^{2+}$ -binding sites
For each calibrated calcium trace, either peak values or slope values using linear regression were analyzed.